Palaeogeography, Palaeoclimatology, Palaeoecology 532 (2019) 109266

Contents lists available at ScienceDirect

Palaeogeography, Palaeoclimatology, Palaeoecology

journal homepage: www.elsevier.com/locate/palaeo

Paleoproterozoic (ca. 1.9 Ga) megascopic life on land in Western Australia

Gregory J. Retallack[a,*], Xuegang Mao[b]

[a] Department of Earth Science, University of Oregon, Eugene, OR 97403-1272, USA
[b] Institute of Geography, Fujian Normal University, Fuzhou 350007, China

ARTICLE INFO

Keywords:
Stirling Range Formation
Paleosol
Paleoclimate
Mycetozoa
Microbial earth

ABSTRACT

Controversial hairpin-shaped trace fossils (*Myxomitodes stirlingensis*) and discoid fossils (*Cyclomedusa davidi*) are here reinterpreted in a reassessment of sedimentology and paleosols of the 1.9 ± 0.1 Ga Stirling Range Formation of Western Australia. Paleosols in the Stirling Range Formation were recognized from complex cracking patterns (peds and cutans), chemical and mineralogical zonation (soil horizons), and poikiloblastic crystals (desert roses). Redox profiles of the paleosols are evidence of well-drained profiles of a coastal plain under a low oxygen (433 ± 116 ppmv) and carbon dioxide (564 ± 64 ppmv) atmosphere. Gypsum pseudomorphs in paleosols that are deeply weathered chemically, represent a persistence of acid sulfate weathering, better known in Archean paleosols before the Great Oxidation event at 2.45 Ga. Chemical composition of the paleosols is evidence of a humid (1478 ± 182 mm mean annual precipitation) temperate (11.3 ± 0.5 °C mean annual temperature) paleoclimate. Their paleoenvironmental setting was a coastal plain on a passive tectonic margin. Megafossils were found on paleosols of western red sandstones of the Stirling Range Formation, not in gray shales and sandstones of marine facies to the east. Trace fossils (*Myxomitodes stirlingensis*) and discoid fossils are both found at the surface of well drained paleosols, and so were not metazoan trails, nor sea jellies. *Myxomitodes* was more likely a grex ("slug") trail of soil slime molds, and the *Cyclomedusa* discoids, were probably microbial colonies. Pervasive microfilamentous structures in the paleosol surface are additional evidence of Paleoproterozoic microbial earth ecosystems.

1. Introduction

Paleoproterozoic (ca. 1.9 Ga) hairpin-like trace fossils of *Myxomitodes stirlingensis* (Bengtson et al., 2007) have been controversial as the oldest complex, and thus eukaryotic, fossils visible with the naked eye. That distinction has been eclipsed by 2.2 Ga terrestrial *Diskagma* (Retallack et al., 2013), 2.1 Ga intertidal-marine Franceville biota (El Albani et al., 2010, 2014, 2019), and perhaps 1.9 Ga lacustrine *Grypania* (Han and Runnegar, 1992; redated by Schneider et al., 2002), but their affinities remain problematic. *Myxomitodes* and associated *Cyclomedusa* discoid fossils were first compared with supposed marine animal "Ediacaran fossils" (Cruse et al., 1993; Cruse and Harris, 1994), or "vendobionts" (Seilacher, 1992, 2007; Fedonkin et al., 2007). Subsequent radiometric dating revealed that they were Paleoproterozoic (ca. 1.9 Ga), much older than the 635–541 Ma Ediacaran Period (Rasmussen et al., 2004). The hairpin-like trails *Myxomitodes* have been attributed to slime molds (Bengtson et al., 2007), marine worms (Rasmussen et al., 2002a), giant aquatic *Gromia*-like protists (Rasmussen et al., 2002b), or wind-driven gas bubbles (Seilacher, 2007). Associated fossil discoid fossils have been interpreted as sea jelly medusae (Cruse et al., 1993; Cruse and Harris, 1994), or as microbial colonies (Grazhdankin and Gerdes, 2007). Our study presents, additional microstratigraphic information on the provenance of fossils within the Stirling Range Formation, in order to assess paleoenvironment and biological affinities of the fossils.

2. Geological setting and age

The Stirling Range Formation of southern Western Australia (Fig. 1), is at least 1600 m thick, and mostly quartz-rich sandstone, with interbedded shales (Muhling and Brakel, 1985). This weather-resistant unit forms an iconic Australian landscape of conical hills (Fig. 2A), topographically and structurally above, and to the north of, metamorphic rocks of the Albany Mobile Belt to the south, from which it is separated by a major east-west fault (Fig. 1). To the north, the Stirling Range Formation unconformably overlies high-grade metamorphic rocks of the Archean Yilgarn Craton (Muhling and Brakel, 1985). Sedimentary structures have been used to infer fluvial, intertidal and shallow marine paleoenvironments (Cruse et al., 1993; Cruse and Harris, 1994; Bengtson et al., 2007). Planar and trough cross bedding indicates

* Corresponding author.
E-mail address: gregr@uoregon.edu (G.J. Retallack).

https://doi.org/10.1016/j.palaeo.2019.109266
Received 8 March 2019; Received in revised form 5 July 2019; Accepted 6 July 2019
Available online 09 July 2019
0031-0182/ © 2019 Elsevier B.V. All rights reserved.

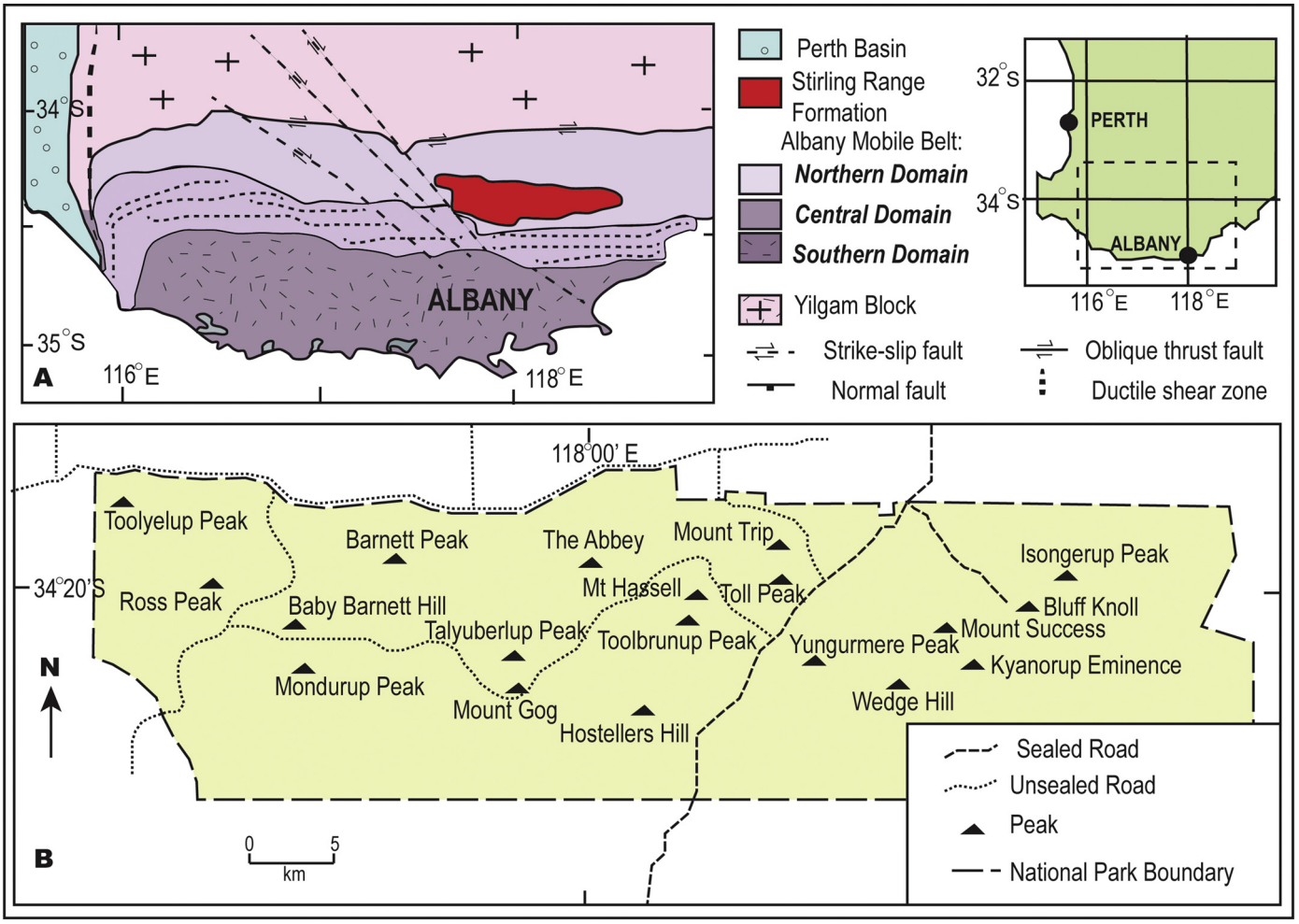

Fig. 1. Geological map and study localities of the Stirling Range Formation (1.9 Ga) in southwestern Australia (modified from Cruse and Harris, 1994).

paleocurrents from the west and southwest (Bengtson et al., 2007). Together with quartz-rich composition, and detrital xenotime and zircon ages (Rasmussen et al., 2004), this indicates provenance from the Yilgarn Craton to the north. The Stirling Range Formation thus formed on a passive continental margin predating deformation, metamorphism, and uplift of the Albany Mobile Belt to the south, which sutured the conjoined Yilgarn-Pilbara Craton to the Mawson (Gawler-East Antarctic) Craton (Dawson et al., 2002, 2003; Rasmussen and Muhling, 2007) into the supercontinent of Rodinia (Evans, 2009).

The Stirling Range Formation was considered Proterozoic in age because unfossiliferous and greenschist rather than amphibolite facies metamorphism (Woolnough, 1920), but discovery of discoid fossils later suggested an Ediacaran age (635–542 Ma: Cruse et al., 1993; Cruse and Harris, 1994), and subsequent deformation during a Pan-African assembly of Gondwana (Harris and Beeson, 1993; Harris, 1994). This was untenable because Turek and Stephenson (1966) had already obtained Rb–Sr metamorphic ages of 1124 Ma and depositional ages of 1340 Ma, in accord with a tectonothermal event during Rodinian assembly at 1300–1140 Ma inferred from Rb–Sr whole rock and U–Pb zircon analyses of gneiss, granite and metasediment elsewhere in the Albany Mobile Belt (Black et al., 1993; Clark et al., 1999, 2000). Dolerite dikes intruding the Stirling Range Formation had been considered Cambrian-Ordovician based on paleomagnetic inclination (Harris and Beeson, 1993; Harris and Li, 1995), but these too proved to be much older, at 1218 ± 3 Ma from SHRIMP U–Pb dating of zirconolite (Rasmussen and Fletcher, 2004). There was a possibility that the rocks with Ediacaran-style fossils were unconformable on the older rocks (Cruse and Harris, 1994), but this unconformity eluded detailed mapping (Bengtson et al., 2007). Instead, SHRIMP U–Pb dating indicated metamorphic monazite rims dated to 1.2 Ga around cores of 1.9–2.6 Ga detrital monazite (Rasmussen et al., 2002a). Finally, SHRIMP U–Pb dating of detrital xenotime grains (3120–2100 Ma) and detrital zircon grains (3460–1960 Ma), and of xenotime overgrowths of two distinct populations (1800 ± 14 Ma and 1662 ± 15 Ma), suggest an age of the Stirling Range Formation between 2.0 and 1.8 Ga (Rasmussen et al., 2004; Rasmussen and Muhling, 2007).

3. Materials and methods

Fieldwork involved observations and collections on Mondurup, Barnett Peak, Tondurup, Mt. Hassell, and Bluff Knoll, and a detailed section was measured on Barnett Peak (Fig. 4), where most of the fossils had been found. The sequence included microstratigraphic patterns of texture and color sampled as putative paleosols for laboratory studies of bulk chemical composition, thin section petrography, and mineral composition (Fig. 5). Thin sections were used to quantify grain size (sand/silt/clay) and mineral compositions (quartz, feldspar, mica, opaque, rock fragment) by point counting (500 points) using a Swift automated point counter on a Leitz Orthoplan Pol research microscope. Accuracy of such point counts is ± 2% for common constituents (Murphy, 1983). Major element chemical analysis was used to characterize chemical weathering trends and metamorphic alteration, and determined by XRF at ALS Chemex in Vancouver, Canada. Bulk density was measured from weight in and out of chilled water of untreated and

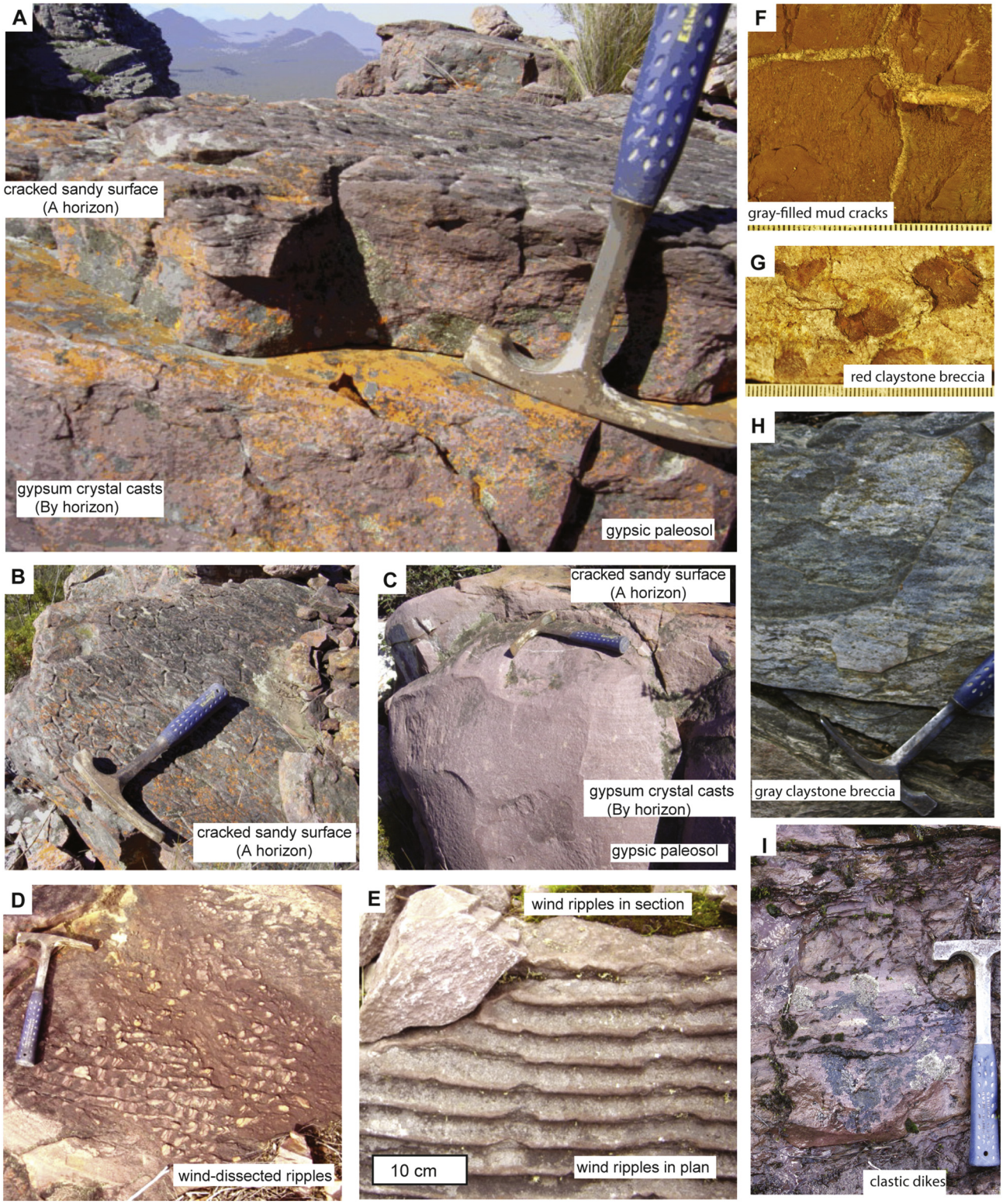

Fig. 2. Field photos of prospective paleosols and sedimentary structures of exposure in the ca. 1.9 Ga Stirling Range Formation of Barnett Peak (A–D, F, I), summit of Mondurup (G specimen R3818) and south saddle of Toolbrunup Peak (E). Hammer for scale has handle 25 cm long, graduations in image F and G are in mm. Stratigraphic levels in Barnett Peak section (Fig. 4) are 85 m (A–B), 80 m (C), 5 m (D), 2 m (F specimen R3817), and 20 m (I).

then paraffin-coated clods (Retallack, 1997). Rare earth element analyses were normalized to post-Archean Australian sediments (Nance and Taylor, 1976). A Cameca SX100 ion microprobe was used for element mapping of polished sections. Rock specimens and thin sections are archived in the Condon Collection of the Museum of Natural and Cultural History of the University of Oregon.

4. Metamorphic and diagenetic alteration

Reconstructing ancient sedimentary environments of metamorphic

rocks requires attention to early diagenetic changes, as well as late diagenetic and metamorphic transformations. Three common early diagenetic alterations are common in the Stirling Range Formation: (1) drab upper portions of beds due to burial gleization of buried organic matter, (2) dark purple-red color from dehydration reddening of ferric hydroxide minerals, and (3) substantial lithostatic compaction (Retallack, 1991). Burial gleization is chemical reduction of oxides and hydroxides of iron by anaerobic bacteria on subsidence below water table, and is especially suggested by drab mottles and tubular features radiating down from bed tops (Figs. 2A,C, 6F,G), well documented in Cambrian (Álvaro et al., 2003; Retallack, 2008) and Proterozoic red beds (Driese et al., 1995; Mitchell and Sheldon, 2009; Retallack, 2013a, 2016a, 2016b).

Also evident is potash enrichment by diagenetic illitization and metamorphic sericitization (Rasmussen and Muhling, 2019), which can be assessed from deviation of chemical analyses toward illite composition and away from a weathering trend toward alumina enrichment (Nesbitt and Young, 1989). Illitization is also indicated by potash mass fraction increase (Novoselov and de Souza Filho, 2015). By both measures, the Stirling Range Formation has suffered significant illitization and sericitization, with compositions clustering around illite (Fig. 3A), and significant potash assays in many samples (Fig. 3B). Because of the strong covariance of alumina and potash (Fig. 3B), illitization can be attributed to retention of potash in clays dewatered of other alkalies and recrystallized by Ostwald ripening, rather than due to introduction of potash in hydrothermal or groundwater solutions (Eberl et al., 1990; Novoselov and de Souza Filho, 2015). Illitization and late diagenetic dewatering may also explain the very low analytical values for calcium, which may have been there in gypsum sand crystals now pseudomorphed by silica (Figs. 2C, 6H). Silicification by silica derived from burial pressure solution (McBride, 1989) is also likely for these sand crystal pseudomorphs.

Rasmussen and Muhling (2019) have made a provocative case for metamorphic oxidation of the Stirling Range Formation from what they presume was a gray protolith rich in organic fragments observed in thin section along with hematite within diagenetic rims of monazite around detrital monazite grains. The rims themselves are evidence against this, because monazite dissolves under oxygen fugacity above the fayalite-magnetite-quartz buffer, which in turn is about 5 orders of magnitude less oxygen than above the magnetite-hematite buffer needed to produce observed hematite (Trail, 2018). Metamorphic oxidation has also been challenged from the perspective of diffusion rates and times in such low permeability rocks (Robbins et al., 2019). The Stirling Range hematite grains may have been recrystallized, reoriented into cleavage, and paleomagnetically reset by metamorphism, but were more likely engulfed by later monazite, and not oxidized during diagenesis or metamorphism, because of the following observations. Red hematite-rich clayey clasts are common in green sandstones (figs 2G, 6B, see also fig 5C of Rasmussen and Muhling, 2019) in the western Stirling Ranges, but gray clasts in gray sandstones remain in the eastern Stirling Ranges (Fig. 2H). Unoxidized coarse grained matrix to these fine-grained hematite-bearing clasts is evidence against pervasive oxidation during metamorphism, because permeable rocks of coarse grain size would be more oxidized than fine-grained rocks by oxidizing fluids, the opposite of observation. Pervasive oxidation, with gray sandstone filling mud cracks (Fig. 2F), local burial gleization around filamentous organic matter (Figs. 2A,C, 6F,G, see also fig 2C of Rasmussen and Muhling, 2019), and varied ferrous/ferric iron ratios (Fig. 5), are comparable with many other examples of Proterozoic red beds (Dreise et al., 1995; Álvaro et al., 2003; Retallack, 2013a, 2016a, 2016b).

The Stirling Range Formation has undergone two generations of folding, formation of multiple cleavages, and is sliced into several northward thrust sheets, yet most exposures have low (5–28°) dips and gentle upright folds (Boulter, 1979; Muhling and Brakel, 1985). Shaley beds of the Stirling Range Formation are mainly sericite and muscovite, with chlorite in cleavage fractures, and biotite limited to isolated rare flakes (Rasmussen and Muhling, 2019). Metamorphic paleotemperatures calculated from Stirling Range Formation chlorites of Barnett Peak are unlikely maxima, because all iron was assumed ferrous despite abundant hematite, but found peak temperatures of 368 ± 56 °C for Fe-chlorites, and 288 ± 36 °C for later Mg-chlorites (Rasmussen and Muhling, 2019). A temperature of 400 °C would give burial depth of 10 km at the 40 °C/km maximum used in Himalayan geothermal calculations (McQuarrie et al., 2014). This is unlikely, because three clastic dikes at 20.5 m in the measured section (Fig. 2I) are compacted to only 73 ± 2% of their ptygmatically folded length, and this corresponds to burial depth of 0.85 km using an equation (Table 1) of Sheldon and Retallack (2001). A single thick clastic dike with sandstone fill at 32.1 m is compacted to 82%, corresponding to 0.49 km burial. Thus the 98 m measured section was in the upper half of the observed 1.6 km of Stirling Range Formation to the east (Muhling and Brakel, 1985), and observed heating at 1.2 Ga was not simply due to

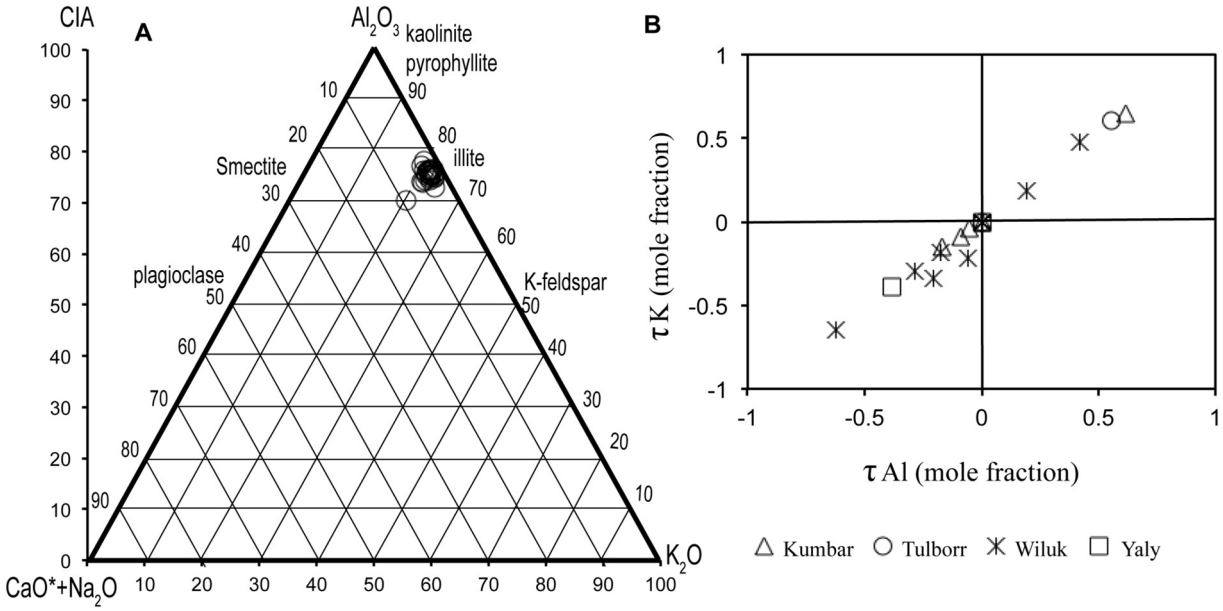

Fig. 3. Geochemical indication of illitization from major element composition (A) and tau analysis (B).

Table 1
Transfer functions used to interpret Stirling Range Formation paleosols.

Equation	Variables	Coefficient (R^2)	Standard error	Reference
$D = \frac{\ln\left[\frac{F_o}{\left(1-\frac{S_i}{C}\right)}\right]}{k}$	D (km) = depth of burial; F_o (fraction) = intial porosity; S_i (fraction) = initial solidity; C (fraction) = compaction; k (material-specific curve-fitting constant) = 0.39 for shaley sand.	None	None	Sheldon and Retallack, 2001
$\tau_{j,w} = \left[\frac{\rho_w \cdot C_{j,w}}{\rho_p \cdot C_{j,p}}\right][\varepsilon_{i,w} + 1] - 1$	$\tau_{w,j}$ (mole fraction) = mass transfer of a specified (j) element in a soil horizon (w); ρ_w (g.cm^{-3}) = bulk density of the soil; ρ_p (g.cm^{-3}) = bulk density of parent material; $C_{j,w}$ (weight %) = chemical concentration of an element (j) in a soil horizon (w); $C_{p,w}$ (weight %) = chemical concentration of an element (j) in the parent material (p): $\varepsilon_{i,w}$ (mole fraction) = strain due to soil formation	None	None	Brimhall et al., 1992
$\varepsilon_{i,w} = \left[\frac{\rho_p \cdot C_{i,p}}{\rho_w \cdot C_{i,w}}\right] - 1$	$\varepsilon_{i,w}$ (mole fraction) = strain of a soil horizon (w) with respect to a stable chemical constituent (i); ρ_w (g.cm^{-3}) = bulk density of a soil horizon; ρ_p (g.cm^{-3}) = bulk density of parent material; $C_{i,w}$ (weight %) = chemical concentration of stable element (i) in a soil horizon (w); $C_{p,w}$ (weight %) = chemical concentration of stable element (i) in the parent material (p)	None	None	Brimhall et al., 1992
$CO_2 = \frac{M}{A\left[\frac{K_{CO_2} P}{1000} + \kappa\frac{D_{CO_2}\alpha}{L}\right]}$	pCO_2 (atmospheres) = partial pressure of atmospheric carbon dioxide: M (mol CO_2/cm$_2$) = summed mass transfer losses of MgO, CaO, Na_2O and K_2O through the profile $M = 2\sum \rho_p \frac{C_{j,p}}{100} \int_{Z=0}^{Z=D_{j,w}} \tau_{j,w(z)}\delta Z$; ρ_p (g.cm^{-3}) = bulk density of parent material; $C_{j,p}$(weight %) = chemical concentration of an element (j) in parent material (p); $\tau_{j,w}$ (mole fraction) = mass transfer of a specified (j) element in a soil horizon (w); Z (cm) = depth in soil represented by analysis; A (years) = duration of soil formation; K_{CO_2} (mol./kg.bar) = Henry's Law constant for CO_2 (=0.034, range 0.031–0.045); P (cm) = mean annual precipitation; κ (s.cm^3/mol.year) = seconds per year divided by volume per mole of gas at standard temperature and pressure (=1409); D_{CO_2}(cm^2/s) = diffusion constant for CO_2 in air (=0.162 at 20 °C, range at 0-40 °C of 0.139–0.181); α (fraction) = ratio of diffusion constant for CO_2 in soil divided by diffusion constant for CO_2 in air (=0.1, range 0.08–0.12); L (cm) = original depth to water table (after decompaction, B below)			Sheldon, 2006
$O_2 = \frac{F}{A\left[\frac{K_{O_2} P}{1000} + \kappa\frac{D_{O_2}\alpha}{L}\right]}$	pO_2 = partial pressure of atmospheric oxygen (atmospheres); F (mol CO_2/cm$_2$) = summed mass transfer gains of Fe_2O_3 through the profile $M = 2\sum \rho_p \frac{C_{j,p}}{100} \int_{Z=0}^{Z=D_{j,w}} \tau_{j,w(z)}\delta Z$; ρ_p (g.cm^{-3}) = bulk density of parent material; $C_{j,p}$(weight %) = chemical concentration of an element (j) in parent material (p); $\tau_{j,w}$ (mole fraction) = mass transfer of a specified (j) element in a soil horizon (w); Z (cm) = depth in soil represented by analysis; A (years) = duration of soil formation; K_{O_2}(mol./kg.bar) = Henry's Law constant for O_2 (=0.00125, range 0.0012–0.0013); P (cm) = mean annual precipitation; κ (s.cm^3/mol.year) = seconds per year divided by volume per mole of gas at standard temperature and pressure (=1409); D_{O_2}(cm^2/s) = diffusion constant for O_2 in air (=0.203 at 20 °C, range from 0 to 40 °C is 0.179–0.227); α (fraction) = ratio of diffusion constant for O_2 in soil divided by diffusion constant for O_2 in air (=0.2, range 0.09–0.32); L (cm) = original depth to water table (after decompaction, B below)			Retallack, 2018
$A = 3920{\cdot}S^{0.34}$	A (yrs) = duration of soil formation; S = diameter of micritic low-magnesium calcite nodules (cm$^-$)	0.57	± 1800 myrs	Retallack, 2005
$A = 3987{\cdot}G + 5774$	A (yrs) = duration of soil formation; G = proportion of surface covered by gypsum crystals or nodules (%)	0.95	± 15,000 yrs	Retallack, 2018
$B = \frac{-0.51}{\frac{0.49}{e^{0.27D}} - 1}$	B (fraction) = compaction of Inceptisol due to burial; D (km) = depth of burial	None	None	Sheldon and Retallack, 2001
$CIA = 100.\ M$	CIA (percent) = chemical index of alteration; M (mole fraction) = $mAl_2O_3/(mAl_2O_3 + mCaO + mNa_2O + K_2O)$.	None	None	Nesbitt and Young, 1989
$P = 221e^{0.0197R}$	P (mm) = mean annual precipitation; R (mole fraction) = $100mAl_2O_3/(mAl_2O_3 + mCaO + mNa_2O)$	0.72	± 182 mm	Sheldon et al., 2002
$T = 0.21R - 8.93$	T (°C) = mean annual paleotemperature; R (mole fraction) = $100mAl_2O_3/(mAl_2O_3 + mCaO + mNa_2O)$	0.81	± 0.5 °C	Óskarsson et al., 2012

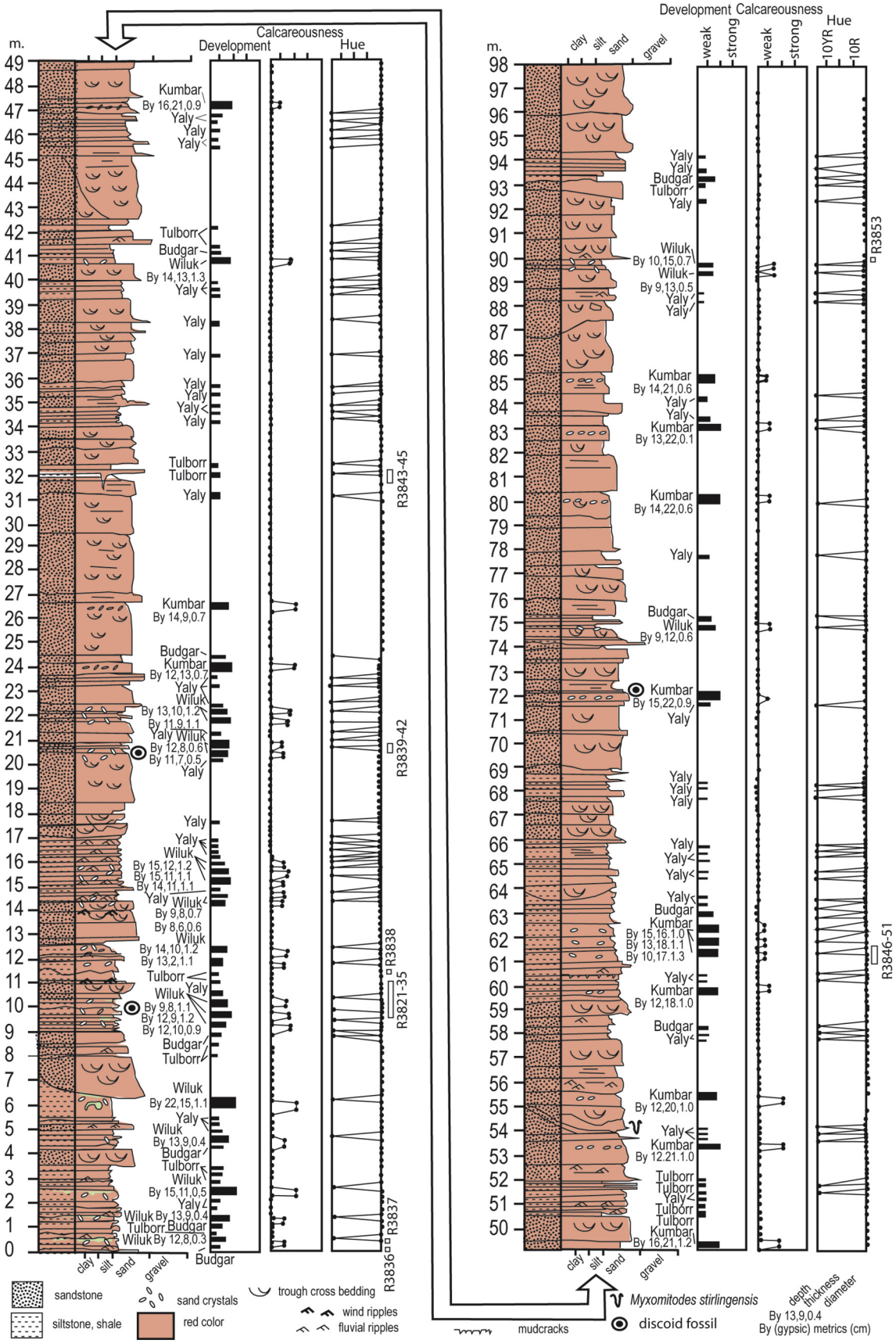

Fig. 4. Measured section of Stirling Range Formation on Barnett Peak. Pedotype names are to the left of the development boxes (black rectangular boxes), based on the soil maturity (Retallack, 2001). Calcification as a guide to aridity is based on field reaction with dilute HCl (Retallack, 2001). Hue as a guide to waterlogging is based on Munsell Color Chart.

burial, but from coeval intrusion of Albany Granite to the south (Turek and Stephenson, 1966).

5. New observations of the Stirling Range Formation

Bengtson et al. (2007) interpret the sedimentary environment of the Stirling Range Formation as tidal flat, coastal plain and shallow marine, but our observations revealed a variety of features unexpected in marine-influenced environments within the same measured section of Barnett Peak. These features, are described and then interpreted in each of the following sections, and apply only to red beds of Barnett Peak, Mondurup, and the tops of Toolbrunup and Mt. Hassell. The various intertidal to marine facies envisaged by Bengtson et al. (2007) were confirmed by examination of gray parts of the Stirling Range Formation on Bluff Knoll, and the lower parts of Toolbrunup and Mt. Hassel.

5.1. Crack patterns

Red beds of the Stirling Range Formation include multiple horizons of shrinkage cracks (Fig. 2A–B, F), which have the v-shaped profile of true desiccation cracks in clay (Weinberger, 2001). These cracks also emanated from the most hematite-rich upper portions of sandy beds, which were the most oxidized (Fig. 2A–C,H). Some cracks had displacive fabric, where a portion of the surface rotated into a cavity under low confining pressure (Fig. 6C), unlike sheared cracks formed during deep burial or metamorphism. The cracks are also complex, with enterolithic deformation of sandstone fill (Fig. 6F,G), collapsing into open spaces.

These v-shaped cracks evidently opened and closed many times, as in a soil alternately wet and dry. A comparable phenomenon is oscillating desiccation cracks of modern intertidal flats (Noffke, 2008, 2009) and mukkara structure of Vertisols (Retallack, 1997).

5.2. Sand crystals

Cracked surfaces with bedding obscured by ferruginization are above a subsurface layer with white patches (Fig. 2A, C). The white patches are areas without pervasive red hematite cement and have either the rounded shape of nodules or the elongate shape of monoclinic crystals with many included sand grains (Fig. 6H). The nodules and crystal pseudomorphs are largely silica now (56–91 wt% Table S3), but electron microprobe mapping (Fig. 7) reveals slight enrichment in calcium, rather than barium, magnesium or sodium. This increase in calcium, together with sharp interfacial angles (Fig. 6H), support interpretation of the dissolved salt as gypsum, rather than barite, kieserite, bassanite, or nahcolite common in Precambrian rocks (Retallack, 2014a, 2018; Retallack et al., 2016; Retallack and Noffke, 2019).

Sand crystals differ from marine or lacustrine evaporites in which the force of crystallization from an extended aqueous medium creates clear crystals without inclusions (Renaut and Tiercelin, 1994; Ziegenbalg et al., 2010). Arrangement of sand crystals in a diffuse horizon below the truncated upper surface of beds is comparable with gypsic horizons of desert soils (Retallack and Huang, 2010). The abundant included quartz grains within crystal pseudomorphs are comparable with desert roses or sand crystals of gypsic soils (Jafarzadeh and Burnham, 1992; Almohandis, 2002).

5.3. Ripple and scour marks

Ripple marks in the Stirling Range Formation are of three main types (Bengtson et al., 2007): (1) straight-crested asymmetric, with sinuous profile, (2) straight to scalloped with symmetrical profile, and (3) straight-crested strongly asymmetric with angular profile (Fig. 2E). In thin section the angular asymmetric type also show inverse grading of laminae characteristic of climbing translatent cross stratification (Fig. 6E).

The first two ripple types are identical to shallow current ripples and oscillation ripples, which form in shallow running and standing water (Allen, 1963; Miller and Komar, 1980). The third angular asymmetric bedforms have climbing translatent cross stratification diagnostic of wind ripples (Allen, 1963; Hunter, 1977; Miller and Komar, 1980). Some of these ripples also show strong orthogonal erosional dissection by wind scouring (Fig. 2D), as noted in other alluvial sandstones (Hocking, 1991; Retallack, 2009a).

5.4. Mineral weathering trends

Beds with sand crystals show surface enrichment of clay and depletion of feldspar (Fig. 4A, C, D) The clay is now illite, but because of burial illitization (Fig. 3), it may not have been entirely illite originally. Other beds not showing these trends (Fig. 4B, D) have thin profiles with relict cross bedding or lamination.

On tidal flats and sea floors, beds can be homogenized by deep burrows, not evident in the Stirling Range Formation, but without coordinated clay gain and feldspar loss. Furthermore, clay formation is asymmetric below sharp grainsize discontinuities and confined to intervals only 5–15 cm thick, unlike alteration by hydrothermal or metamorphic alteration, which would be more diffuse and symmetrical around fluid flow-paths. These combinations of mineral and textural change are evidence of hydrolytic weathering of feldspar to clay in soils with sand crystals and obscured bedding from a long duration of soil formation (Retallack, 2018). Beds with relict bedding and mudcracks by this interpretation, would thus be insufficiently developed to show significant mineral weathering.

5.5. Chemical weathering trends

Molar weathering ratios display abrupt changes between beds, but there also are subtle and consistent changes within beds (Fig. 4A, C, D). There is negligible change in soda/potash and alkaline earths/alumina, and thus no evidence for marine early diagenetic enrichment of alkalies and alkaline earths (halmyrolysis of Clauer et al., 1990; Setti et al., 2004).

Surficial increases in alumina/silica and alumina/ bases at the tops of profiles with sand crystals is evidence, additional to that of mineral trends, for hydrolysis of feldspar to clay within soil profiles. Other profiles with obvious relict bedding and no sand crystals, so formed over a shorter time frame, show more erratic or muted trends in alumina enrichment. Generally high Ba/Sr is evidence of unusually high chemical leaching, but lack of systematic variation of Ba/Sr within profiles can be taken as evidence that this chemical leaching was not so much during the intervals between deposition, as created during formation of the mineralogically mature quartz-rich, sedimentary parent material. Declining ferrous/ferric iron toward the surface of profiles is evidence of surface oxidation, but subsurface chemical reduction (gleization: Retallack, 1997). Negligible changes in soda/potash and alkaline earths/alumina are evidence against salinization or calcification in soils.

5.6. Tau analysis

Molar weathering ratios of alluvial paleosols can be subtle, but a definitive method to disentangle soil formation from sedimentation is tau analysis (Brimhall et al., 1992). This analysis deconstructs two separate aspects of weathering: mass transport ($\tau_{j,\,w}$) of a mobile element and strain ($\varepsilon_{i,\,w}$) of an immobile element (Table 1). Soils and paleosols lose mass with weathering and so have negative strain ($\varepsilon_{i,\,w} < 0$), and also lose nutrient cations and silica, so negative mass transfer ($\tau_{j,\,w} < 0$). In contrast, sediment accumulation and diagenetic alteration other than weathering has positive strain and mass transfer. Tau analysis has been widely used for Precambrian paleosols (Retallack and Mindszenty, 1994; Driese, 2004), as well as Miocene paleosols

(Bestland et al., 1996; Sheldon, 2003), and modern soils (Chadwick et al., 1990; Brimhall et al., 1992; Merritts et al., 1992). On this basis, most analyses of Stirling Range Formation paleosols are within the collapse and loss quadrant, with the exception of two samples, which can be taken as evidence of eolian additions to the surface (Fig. 8).

5.7. Rare earth element analysis

Rare earth chemical analysis of individual beds in the Stirling Range Formation has a slight to negligible negative europium anomaly (Fig. 9), like that of sediments from granitic (Foden et al., 1984), but not mafic rocks (Bavinton and Taylor, 1980) of the Yilgarn Craton to the north. Stirling Range Formation lacks marked enrichment in europium or other rare earth elements found in hydrothermally altered rocks (Bolhar et al., 2005; Sugahara et al., 2010). The even distribution of rare earth elements normalized to post-Archean Australian sediment (Nance and Taylor 1976) is compatible with sandstone mineral compositions of a geologically diverse recycled orogen, like the Yilgarn Craton to the north (Fig. 10).

Within many beds there is overall rare earth element enrichment of surface horizons compared with bases of beds, and also light rare earth enrichment. These trends are most apparent in red beds (Kumbar, Wiluk, Yaly and Tulborr of Fig. 9A–C), but not in red-green mottled beds (Budgar of Fig. 9D), which may have been intermittently waterlogged to form reduction spots (Vepraskas and Sprecher, 1997).

Marine diagenesis of sediments (halmyrolysis) does not change rare earth concentrations significantly over short (10–20 cm) thicknesses (Clauer et al., 1990; Setti et al., 2004). LREE enrichment like that of Stirling Range Formation beds has been observed in Archean alluvial paleosols (Retallack, 2018). Comparable REE enrichment favoring LREE is also seen in modern aridland loessial soils (Ramakrishnan and Tiwari, 1999; Compton et al., 2003), but is distinct from REE depletion seen in humid granitic soils (Kurtz et al., 2001; Aubert et al., 2001; de Sá Paye et al., 2016).

5.8. Biotic microstructures

Surface horizons of the beds chosen for petrographic study do not show stromatolites, rollups, detached mat fragments, or other features of microbial mats in aquatic environments (Noffke, 2009), but rather a variety of features of microbial earth soils (Retallack, 2012). Thin section micromorphology shows tufted and irregular surface organic matter (Fig. 6A–B), and near vertical microtubular structures running across bedding (Fig. 6,D). These are hallmarks of microbial biomass organized to withstand surface disruption, to grow through later layers, and to persist despite surface cracking, comparable with microbial trace fossils documented from Ediacaran to Cambrian paleosols (Retallack, 2008, 2009b, 2011). Microbial earths include a variety of thread-forming, tufted, and globular masses of interstitial microbes (Belnap, 2003).

6. Paleosol interpretation

The preceding paragraphs presented evidence that the western Stirling Range Formation red beds are a sequence of fossil soils, passing eastward into gray marine to intertidal facies at Bluff Knoll, rather than marine rocks oxidized by northward-declining metamorphism only in the west (Rasmussen and Muhling, 2019). The remainder of this paper explores the significance of this conclusion, by assuming that the red beds were paleosols. The various kinds of beds analyzed as putative paleosols have been named (Table 2) using the Nungar aboriginal language (Douglas, 1991). Despite burial illitization and greenschist facies metamorphism, these pedotypes can now be interpreted in terms of soil taxonomy and various soil-forming factors to build a detailed model of the paleoenvironmental setting of fossils in the Stirling Range Formation (Table 3, Fig. 12).

Table 2
Summary of Stirling Range Formation paleosol definition and classification.

Pedotype	Aboriginal meaning	Diagnosis	US taxonomy (Soil Survey Staff, 2014)	Food and Agruiculture Oorganization (1974) map	Old Australian (Stace et al., 1968)	New Australian (Isbell, 1996)
Budgar	Earth	Gray-green siltstone (A) over red motled sandstone (Bw)	Ochrept	Eutric Cambisol (Be)	Brown clay	Brown Dermosol
Kumbar	Big	Cracked "old elephant skin texture" (A) over red sandstone with white crystal pseudomorphs (By)	Gypsid	Orthic Solonchak (Zo)	Desert loam	Gypsic Hydrosol
Tulborr	Fine soil	Gray-green mottled siltstone (A) over red bedded shaley siltstone (C)	Fluvent	Eutric Fluvisol (Je)	Alluvial soil	Stratic Rudosol
Wiluk	Red ochre	Gray-green siltstone (A) over red sandstone with white crystal pseudomorphs (By)	Gypsid	Gleyic Solonchak (Zg)	Desert loam	Gypsic Hydrosol
Yaly	Sand	Gray-green mottled siltstone (A) over red bedded sandstone (C)	Psamment	Eutric Regosol (Re)	Siliceous sand	Arenic Rudosol

Note: Aboriginal definitions are from Nungar aboriginal language (Douglas, 1991).

Table 3
Summary of Stirling Range Formation paleosol interpretation.

Pedo-type	O_2 (ppm)	CO_2 (ppm)	Paleoclimate	Organisms	Topography	Parent material	Soil duration (yrs)
Budgar	Not known	Not known	Humid (MAP 1415 ± 182 mm) temperate (MAT 10.9 ± 0.5 °C)	Microbial earth	Well-drained floodplain	Clayey silt	500
Kumbar	433 ± 116	564 ± 64	Humid (MAP 1509 ± 182 mm) temperate (MAT 11.5 ± 0.5 °C)	Large microbial colony (*Cyclomedusa davidi*)	Well-drained levee	Quartzofeld-spathic sand	3772 ± 1800
Tulborr	Not known	Not known	Not known	Slime mold (*Myomitodes stirlingensis*)	Seasonally wet floodplain swale	Clayey silt	100
Wiluk	Not known	Not known	Humid (MAP 1493 ± 182 mm) temperate (MAT 11.4 ± 0.5 °C)	Small microbial colony (*Cyclomedusa davidi*)	Well drained floodplain	Clayey silt	3690 ± 1800
Yaly	Not known	Not known	Not known	Microbial earth	Well drained levee	Quartzofeld-spathic sand	100

6.1. Paleosol identification

Beds with cracked surface (A horizon) over a diffuse horizon with mottles and sand crystsls (By or gypsic) are most like Gypsids (Soil Survey Staff, 2014). Comparable considerations can be used to classify the paleosols in classifications of Australia (Stace et al., 1968; Isbell, 1996) and of the Food and Agriculture Organization (1974). Classification of Kumbar paleosols in the FAO system as a Solonchak (among others in Table 2) allows use of modern soil maps to find modern soilscapes comparable with the Stirling Range paleosol assemblage, which can be described by the FAO code as Zo with inclusions of Zg, Jd, and Rc (Orthic Solonchak, with Gleyic Solonchak, Dystric Fluvisol and Eutric Regosol). A match to this is map unit Zo36-2a, with associated Zg, and inclusions of Rc, Rd, Xk and Yh (Calcaric Regosol, Dystric Regosol, Haplic Xerosol, and Haplic Yermosol) widespread in Western Australia from Lake Disappointment in the Pilbara region south to Lake Lefroy in the Yilgarn region (Food and Agriculture Organization, 1978). These distinctive soils range from regions of desert shrubland into the formerly wooded “wheat belt”, under a mean annual precipitation range of 260–340 mm (Benison and Bowen, 2013, 2015). This region has mean annual temperature of 18–20 °C (Bureau of Meteorology, 2016). These parts of Western Australia have a mix of desert soils developed on siliceous sands, as well as lateritic residuum from thick Ultisol and Oxisol paleosols of the Miocene (McKenzie et al., 2004). These Solonchak soils are also called “acid saline lakes” (Benison et al., 2007; Benison and Bowen, 2013), even though dry more often than flooded. Despite abundant salts, these lakes have very acidic waters (pH 1.4–3.9), due to oxidation of sulfides unbuffered by carbonate in soils or bedrock (Benison and Bowen, 2015). Halite and gypsum are the principal evaporite minerals (Benison and Bowen, 2013).

6.2. Original parent material

Parent materials to the paleosols were mostly sands and silts of arkosic composition, with the feldspars dominated by K-felspar. Biotite and muscovite mica also was prominent in the sands and silts. Clays are mainly illitic, and all the sediments show a high chemical index of alteration (Fig. 3). These sediments were from a low relief, granitic-metamorphic terrain of the Yilgarn Craton to the north. This was evidently not a deeply weathered terrain with Oxisols as it is today (McKenzie et al., 2004), because the Stirling Range Formation lacks kaolinite, gibbsite, or boehmite.

6.3. Reconstructed sedimentary setting

Our analysis of putative paleosol beds does not support the interpretation of red beds on Barnett Peak as marine offshore, tidal inlets, tidal flats, and flood tidal deltas by Bengtson et al. (2007), although we do recognize intertidal facies and found no paleosols in gray shales and sandstone of Bluff Knoll to the east. The mud-draped gutter detailed by Bengtson et al. (2007, fig. 4–5) and here (Fig. 11A), was thus not intertidal, but a fluvial levee swale. We support the interpretation of Cruse et al. (1993; Cruse and Harris, 1994) of an array of eolian, fluvial, intertidal, and shallow marine paleoenvironments. To the east near Bluff Knoll and Toolbrunup are gray tidalite and turbidite facies, whereas to the west near Barnett Peak are red beds with trough cross-bedded sandstones filling what appear to be fluvial paleochannels. Toolbrunup and Mt. Hassell also have eolian ripples and paleosols in red beds near the summits (Fig. 2E), but gray sandstones and shales below, so that the paleoshoreline was near a current longitude of 118°E.

Within this coastal plain, Wiluk and Kumbar paleosols have sand crystals as evidence of floodplains that were stable for millennia. All the paleosols were oxidized and well drained, because red with pervasive hematite. Although there are Cenozoic lateritic paleosols (Woolnough, 1920; Muhling and Brakel, 1985), notably around the carpark below Bluff Knoll, lateritization is not responsible for red color of the Stirling Range Formation because paleosol clasts have remained red within light gray sandstone on Tondurup, Barnett Peak, and Mondurup (Fig. 2G). Kumbar paleosols lack the surface drab mottles of Wiluk paleosols. Thus, Kumbar profiles were well drained, but Wiluk paleosols formed in parts of floodplains that suffered burial gleization when subsiding below a shallow water table (Retallack, 1991). Water table was at least 15 cm deep in Wiluk paleosols, judging from ptygmatically folded clastic dikes, and at least 20 cm in the weakly developed Tulborr profile. The Tulborr profile at the *Myxomitodes* locality is a red shale drape to a small erosional swale with relief of a meter into channel sandstone (Bengtson et al., 2007). The swale was part of a channel margin, which also included weakly developed Budgar and very weakly developed Yaly profiles in areas with high water table, leaving drab mottles due to burial gleization (Retallack, 1991).

6.4. Time for formation

Clear relict bedding in Tulborr and Yaly pedotypes marks them as very weakly developed, and modest destruction of bedding in Budgar paleosols are evidence of weakly developed profiles, which form in as little as 100 to 1000 years (Retallack, 2001). Chronofunctions of modern aridland soils can be used to constrain time for formation of Wiluk and Kumbar profiles. An upper limit of 23,111 ± 15,000 yrs (average of 227 with range 20,327–26,147 years) comes from compaction corrected percent surface area of sulfate nodules in Wiluk paleosols, compared with well dated modern aridland soils (Retallack, 2013a) using equations shown in Table 2. Comparable calculations for Kumbar paleosols give 17,624 ± 15,000 yrs (average of 14 with range 14,505–23,237 years). A lower limit of 3690 ± 1800 years (average of 22 with range 2603–4170) comes from diameter of nodules in Wiluk paleosols, compared with calcite nodules in aridland soils (Retallack, 2005). Comparable calculations for Kumbar paleosols gives 3772 ± 1800 yrs (average of 14 with range 3295–4395 years). Neither estimate is satisfactory for a variety of reasons, including differences between sand crystals in the paleosols and nodules in modern soils, and the very different biota of land plants in modern analogs. Nevertheless,

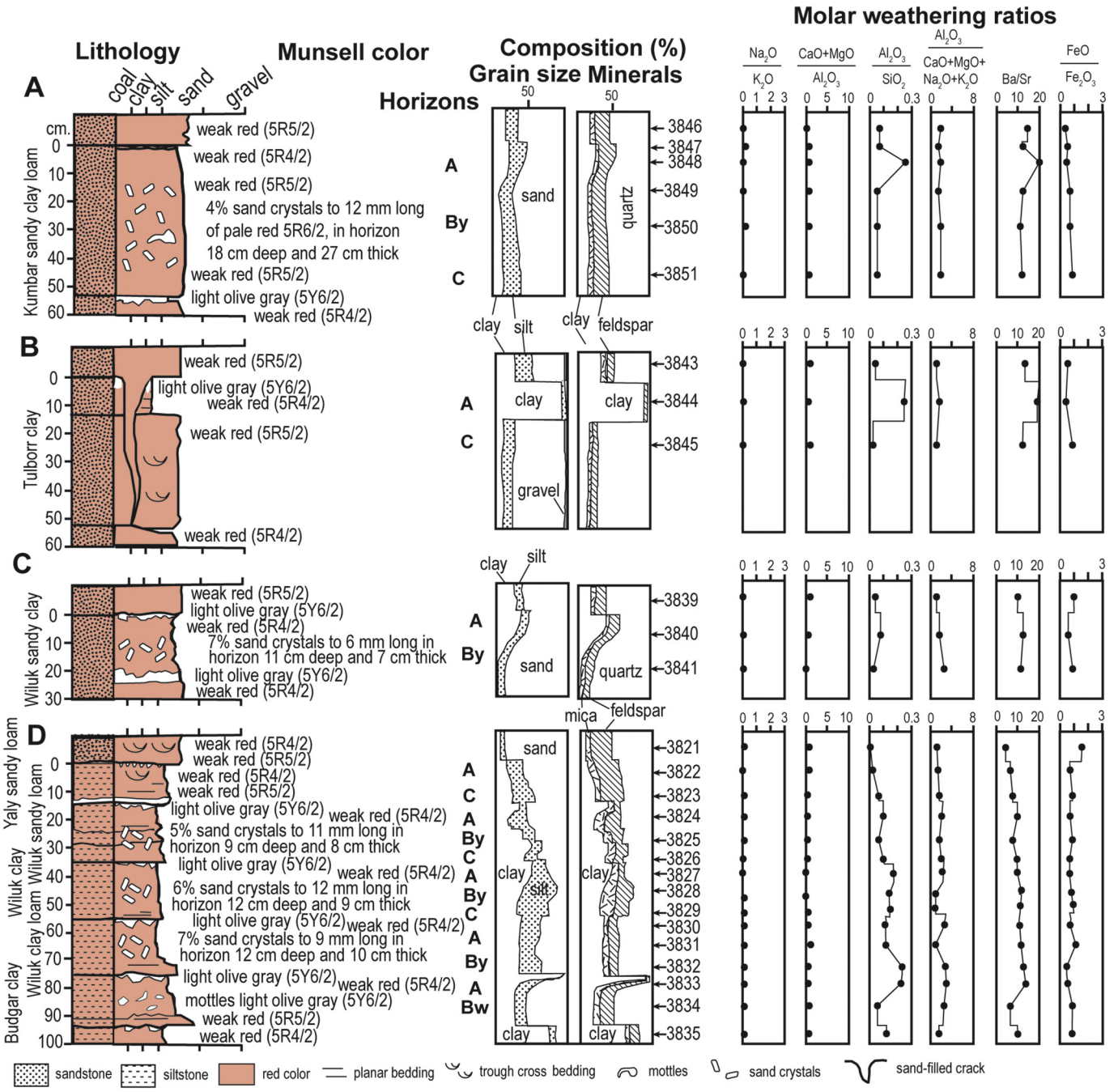

Fig. 5. Field observations, grain size and mineral content by point counting under petrographic thin section, and molecular weathering ratios of pedotypes in Stirling Range Formation.

the millennial exposure times of the nodular paleosols are likely, and the whole sequence of paleosols represents more time than the ephemeral surfaces of tidal deltas and flats envisaged by Bengtson et al. (2007).

6.5. Paleoclimate

Gypsic soils are today mainly found in arid regions where soils are also rich in other nutrient cations (Navarro-González et al., 2003; Ewing et al., 2006), but the paleosols have high chemical index of alteration of humid climate soils (Fig. 3), with much feldspar, and no kaolinite, gibbsite and boehmite of paleosols formed on redeposited Oxisols (Mao and Retallack, 2019). Gypsic horizons form by acid sulfate weathering in modern climates as humid as 1287 mm mean annual precipitation (Retallack and Huang, 2010; Benison and Bowen, 2013, 2015). Archean paleosols rich in gypsum and barite also reveal a paradox of sulfate-rich soils without base-rich composition of aridland soils (Nabhan et al., 2016; Retallack et al., 2016; Retallack, 2018). A better paleoprecipitation proxy for acid sulfate soils is CIA-K chemical composition of B horizons (Sheldon et al., 2002), which removes potash from the normal computation for chemical index of alteration (Table 1), because of likely alteration due to deep burial diagenesis (Fig. 3). This chemical proxy gives mean annual precipitation of 1509 ± 182 mm for the upper Bg horizon of the Kumbar paleosol at 61.5 m in Fig. 4, 1415 ± 182 mm for the Bw horizon of the Budgar paleosol at 8.9 m, and an average of 1493 ± 182 mm for three Bg horizons of Wiluk paleosols at 9.3, 9.8 and 20.5 m.

A rough guide to paleotemperatures is chemical index of alteration

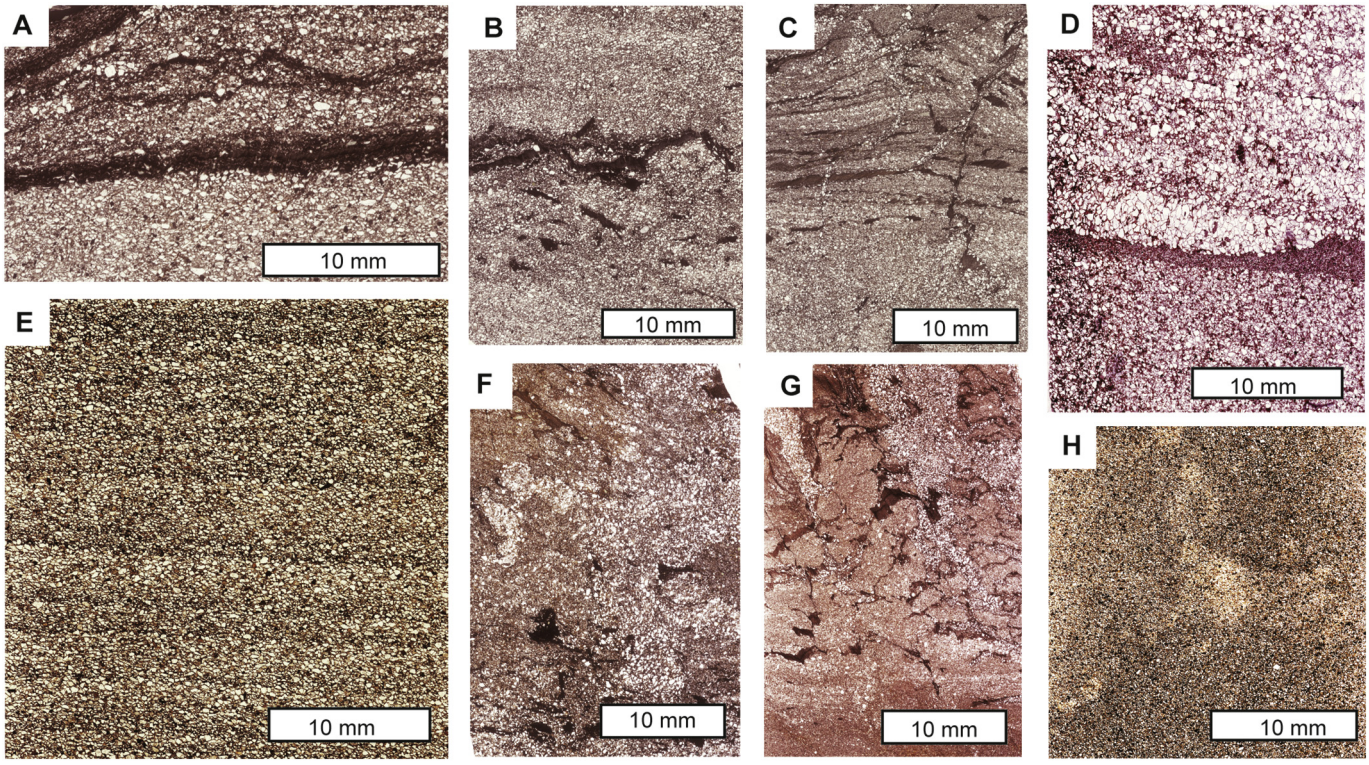

Fig. 6. Petrographic thin sections cut perpendicular to bedding showing discoid fossils in surface horizon (A), mat-controlled desiccation cracks (C), microtubular structures (D), coearsneing upwards eolian beds (E)., surface enterolithic structure (F–G)., and sand crystal pseudomorphs (H) from the Stirling Range Formation. Specimens are R3840 (A), R3823 (B), R3830 (C), R3469 (D), R3845 (E), R3826 (F), R3828 (G), R3850 (H).

(Table 1) which is now < 65% in glacial-frigid climates and > 80% in tropical climates, but between these limits in temperate climates (Nesbitt and Young, 1989). This proxy can be computed for soils and sediments indiscriminately, and for our 26 analyses of the Stirling Range Formation is 76.2 ± 1.2%, which suggests temperate paleoclimate. Other pedogenic paleothermometers are based on soils of modern woody vegetation (Sheldon et al., 2002; Gallagher and Sheldon, 2013) are not applicable to likely microbial earths of Precambrian paleosols (Retallack, 2014b). A paleothermometer based on modern soils under lichen-shrub tundra vegetation of Iceland (Óskarsson et al., 2012) is the best currently available option, predicting temperature (T in °C) from chemical index of weathering (W), which is another base depletion metric (Table 1). This chemical proxy gives mean annual temperature of 11.5 ± 0.5 °C for the upper Bg horizon of the Kumbar paleosol at 61.5 m in Fig. 4, 10.9 ± 0.5 °C for the Bw horizon of the Budgar paleosol at 8.9 m, and an average of 11.4 ± 0.5 °C for three Bg horizons of Wiluk paleosols at 9.3, 9.8 and 20.5 m. These are all temperate paleoclimates.

Equatorial temperatures may have been low during deposition of the Stirling Range Formation in tropical paleolatitudes. The 1.8–1.9 Ga Frere Formation of the northern Yilgarn Craton had a paleolatitude of 13 ± 1.5 °C (Williams et al., 2004). The Frere Formation is 890 km and 8° of latitude north of the Stirling Range, which could have been at a paleolatitude of no more than 21° at 1.8 Ga, depending on plate orientation. The 1.89 Ga Boonadgin dikes of the southwestern Yilgarn Craton also had a paleolatitude of 13 ± 6 °C (Liu et al., 2019), only 200 km and 1.2° latitude north of the Stirling Range.

6.6. Paleoatmospheric carbon dioxide

A modelling approach of Sheldon (2006) for calculating ancient atmospheric CO_2 from paleosols uses measured depletion of cationic bases (Ca^{2+}, Mg^{2+}, Na^{+}, K^{+}) within the paleosol profile, assuming that each electrical equivalent was displaced by hydronium (H^{+}) from carbonic acid. The integrated milliequivalent loss of all four bases within the profile is assumed equal to moles of carbonic acid used over the lifetime of the soil. These calculations are complex, involving also gas constants, and independent estimates of depth to water table, mean annual precipitation, and duration of soil development (Table 1). Gaussian error propagation of so many variables can be done by partial differential equations in quadrature (Supplementary Tables S6–7; Hughes and Hase, 2010). Calculations for the Kumbar paleosol, assuming 3772 years duration of formation (Section 6.4), 150.9 cm mean annual precipitation (Section 6.5), and decompacted depth to water table of 71 cm (Fig. 5A, Table 1), is 564 ± 46 ppm CO_2 (2 PAL, or twice preindustrial atmospheric level).

This is surprisingly low compared with another Paleoproterozoic (2.1 Ga) estimates of atmospheric CO_2 of 6440 ± 194 ppm or 23 PAL (Sheldon, 2006) using the same model for the Waterval Onder paleosol (Retallack et al., 2013), and a comparable but different model yielding 1500–9000 ppmv (5–32 PAL) CO_2 for the Archean (3.0 Ga) Jerico Dam paleosol of South Africa (Grandstaff et al., 1986). This calculation could be improved with more accurate estimates of time for soil formation (Sheldon, 2006). Even the most extreme of these estimates is short of the amount needed for a greenhouse capable of maintaining temperate paleotemperatures given the faint young sun (Fiorella and Sheldon, 2017). Other greenhouse gases are needed, including water vapor, CH_4, C_2H_6, SO_2, and COS (carbonyl sulfide: Kasting and Kirschvink, 2012; Ohmoto et al., 2014). An atmosphere with three times the current mass of N_2 and a H_2 mixing ratio of 0.1, would also have created an adequate greenhouse (Wordsworth and Pierrehumbert, 2013). Overall atmospheric pressures estimated for the late Archean (2.7 Ga) were no > 1.1 bars judging from size of raindrop prints (Som et al., 2012), and no > 0.5 bars judging from basaltic vesicle sizes at sea level (Som et al., 2016). Lower than modern atmospheric pressure and temperate equatorial paleoclimate (Section 6.5) mitigates this greenhouse paradox.

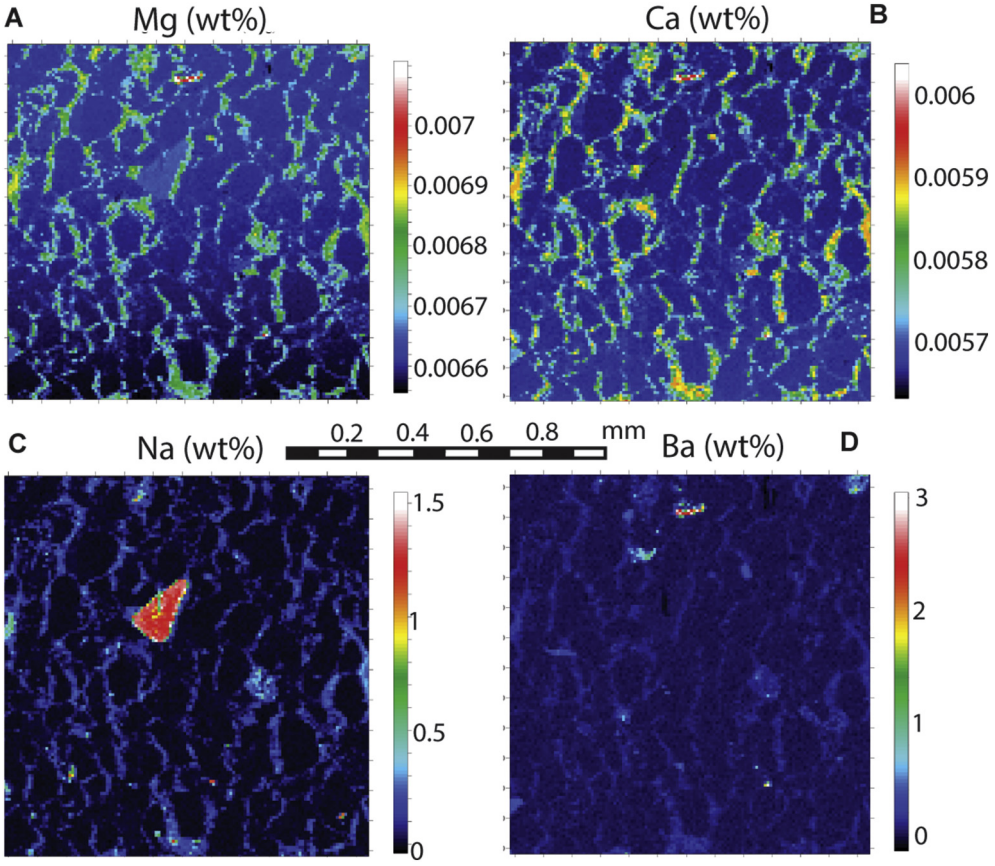

Fig. 7. Microprobe elemental maps of sand crystal pseudomorph in specimen R3850 for (clockwise from top left) Mg, Ca, Ba, Na.

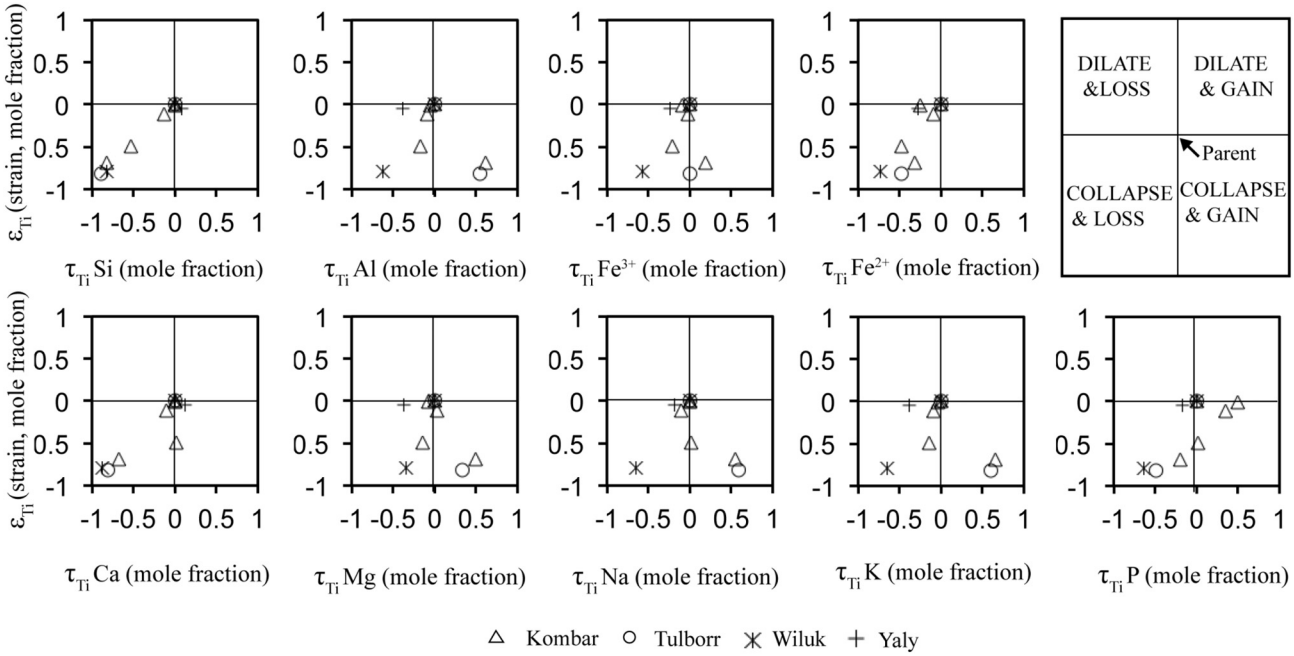

Fig. 8. Mass transport (mole fraction) and strain (mole fraction) plotted as deviation from parent materials at origin within paleosols of the Stirling Range Formation. Strain in soils (y-axis) is usually negative, meaning collapse of volume. Mass transfer (x-axis) in soils is also negative, meaning loss, but can be gain (positive) for redox-sensitive oxides.

6.7. Paleoatmospheric oxygen

Atmospheric O_2 also can be calculated in a comparable way from oxidation and retention of Mn^{4+} and Fe^{3+} (Retallack, 2018). The integrated profile gain of these common redox-sensitive elements are assumed equivalent to the availability of oxygen as an oxidant over the lifetime of the soil. Other variables needed and Gaussian error propagation are comparable to the calculations for CO_2 (Section 6.6), and for

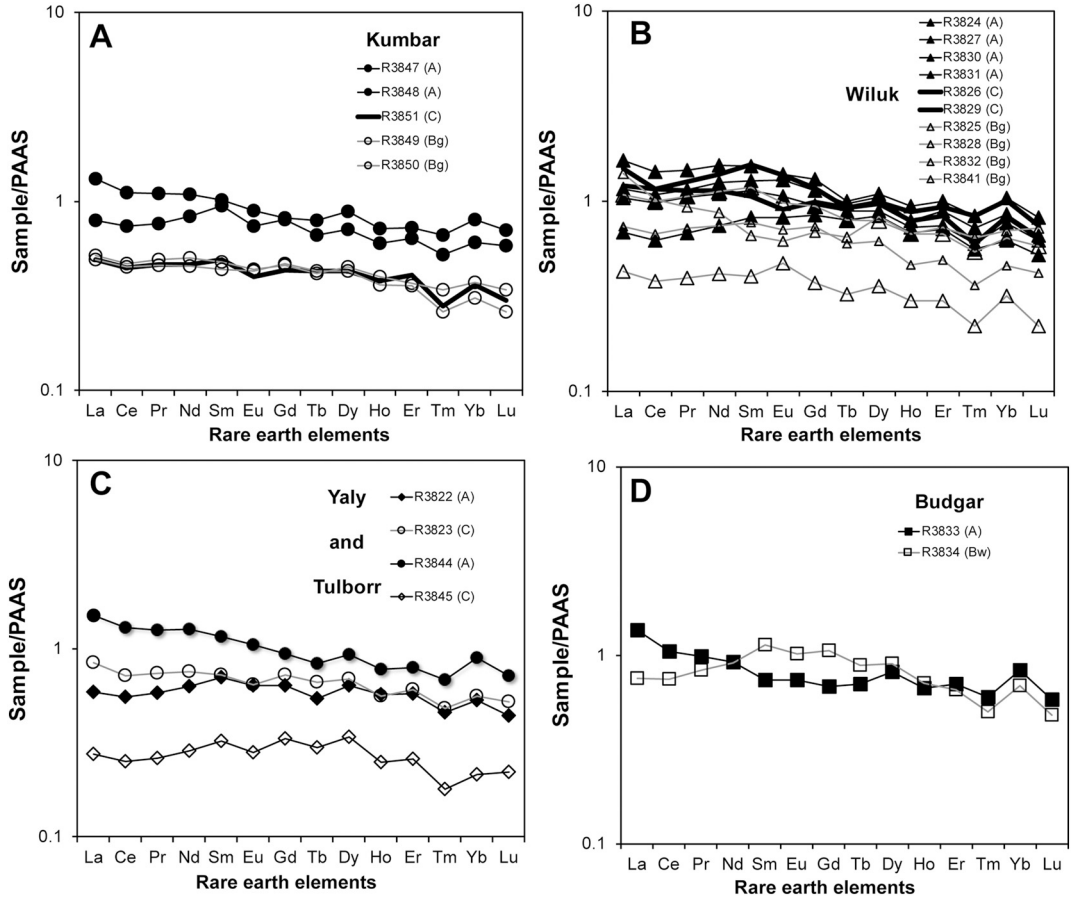

Fig. 9. Rare earth element and trace element distribution patterns of Stirling Range Formation pedotypes.

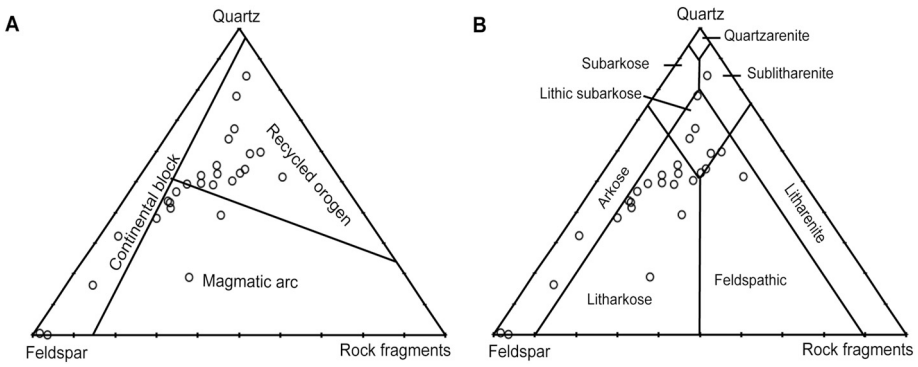

Fig. 10. Tectonic setting (A) and sandstone classification (B) based on point counting of sandstones from the Stirling Range Formation.

the Kumbar paleosol give 433 ± 116 ppm O_2 (0.002 PAL). Very low levels of atmospheric oxygen are indicated by high ferrous to ferric iron ratios of paleosols in the Stirling Range Formation (Fig. 5), comparable with swamp soils today exhausted of oxygen by microbial respiration (Vepraskas and Sprecher, 1997). However, paleosols of the Stirling Range Formation were not waterlogged, as indicated by red color (Fig. 2A–C), and sand crystals of gypsum (Fig. 6H).

These estimates of atmospheric O_2 are very low considering that they postdate the Great Oxidation Event at 2.45 Ga, when O_2 may have risen from 21 to 210 ppm (10^{-7}–10^{-8} PAL) during the Archean, to 2100–84,0000 ppm (0.01–0.4 PAL) during the Paleoproterozoic (Kump, 2008). However, this transition is no longer seen as a simple step function, but a series of oxygenation events corresponding to glaciations and isotopic transients between 2.0 and 2.7 Ga (Lyons et al., 2014), and it is unclear when exactly within these oscillations the Stirling Range Formation was deposited. Widespread marine anoxia, and sedimentary Cr isotopic fractionation are evidence for Paleoproterozoic O_2 levels of < 2100 ppm (Planavsky et al., 2018), compatible with our estimate here. Paleosols in the 1.8 Ga Stirling Range Formation are red with hematite, but also contain much reduced iron (Fig. 5), as is common in Proterozoic paleosols (Planavsky et al., 2018).

6.8. Life on land

Fieldwork in the Stirling Range confirmed geographic distribution of megafossils mainly toward the west: they were seen on Mondurup, Barnett Peak, and near the summits of Mt. Hassell and Toolbrunup, but not in the extensive exposures or rubble of Bluff Knoll. The location of the *Myxomitodes stirlingensis* fossils of Bengtson et al. (2007) on Barnett Peak is 50 m east of the main section line but at a stratigraphic level of

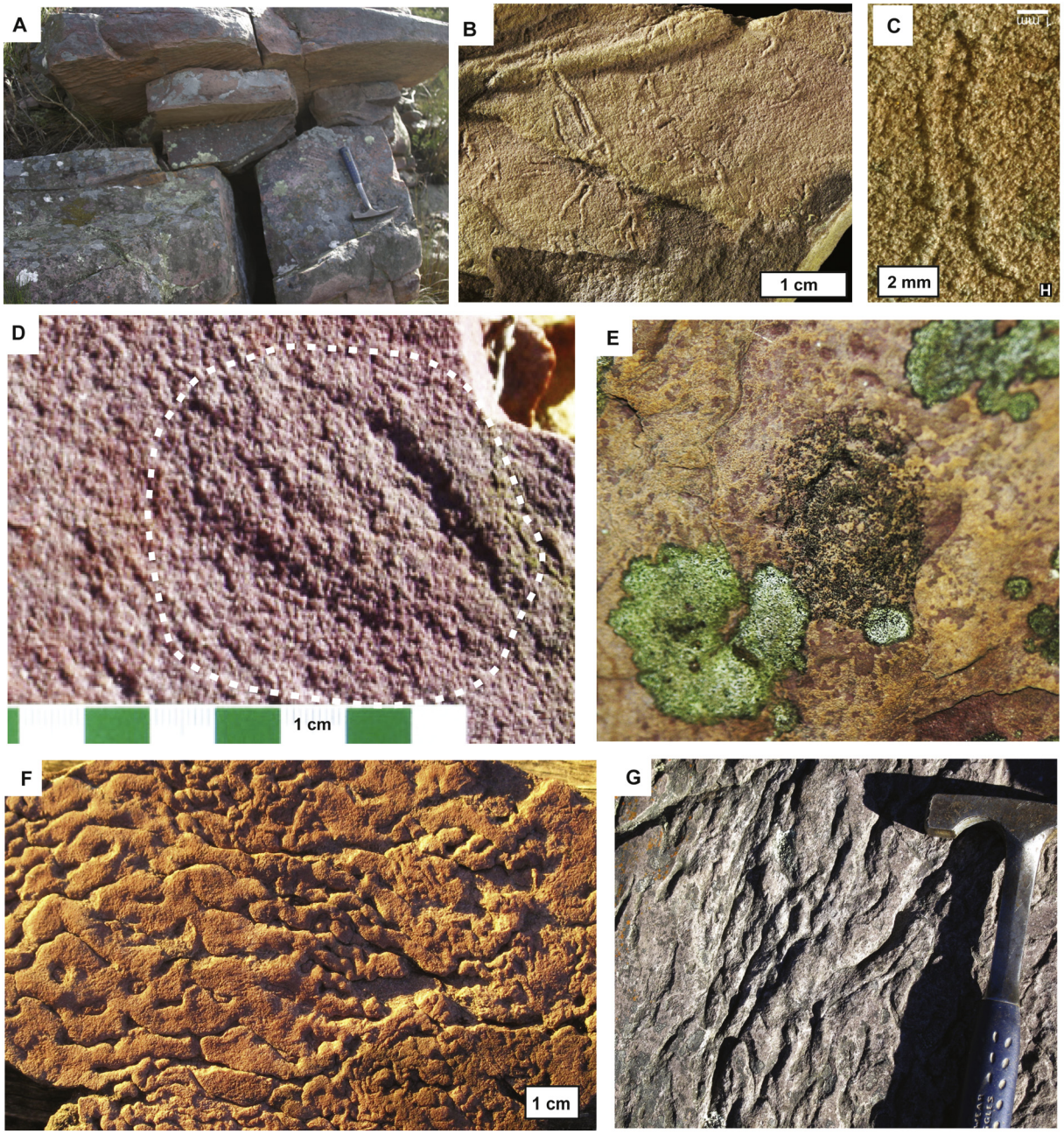

Fig. 11. Fossils from the Stirling Range Formation: clay-lined paleogully (to left of hammer) with *Myxomitodes stirlingensis* at 53.8 m on Barnett Peak (A), hairpin-like trace *Myxomitodes stirlingensis* from Barnett Peak (B–C), discoids *Cyclomedusa davidi* from 75.2 m and 10 m (respectively) on Barnett Peak (D–E), microbially induced sedimentary structure *Rugalichnus matthewi* (F) and *Rivularites repertus* (G) from float on Barnett Peak (F) and summit outcrop of Mt. Hassell (G). Living green crustose lichens in panel E are *Rhizocarpon geographicum*.

54 m. They are in claystones of a Tulborr pedotype lining a shallow (1 m amplitude) erosional swale. Discoids, referred to *Cyclomedusa davidi* by Cruse et al. (1993; Cruse and Harris, 1994), also were found in place at three levels in the measured section: atop Wiluk paleosols at 10 and 20.5 m, and atop a Kumbar paleosol at 72.2 m.

Myxomitodes has been considered the trail of a worm-like metazoan (Rasmussen et al., 2002a), the trace of gas bubbles driven by wind (Seilacher, 2007), the rolling trace of cyanobacterial or algal ball (Rasmussen et al., 2002b; Bengtson and Rasmussen, 2009), or a grex (slug) trail of a slime mold (Bengtson et al., 2007). Our demonstration of a paleosol setting confirms interpretation as slime molds (Mycetozoa), which are usually dispersed amoeboid soil organisms, but aggregate into a slug to move short distances before putting up a sporulating stalk (Bonner, 2015). Other likely fossil slime-mold slug trails have recently been found in the 2.1 Ga Franceville Formation of Gabon (El Albani et al., 2019), and 0.55 Ga Shibantan Member of the Doushantou Formation in China (Retallack, 2013b). Plasmodial slime molds may be represented by the enigmatic *Nilpenia rossi* from the 0.55 Ga Ediacara Member of South Australia (Droser et al., 2014). These are all eukaryotic organisms, but not the oldest soil eukaryotes, which are 2.2 Ga *Diskagma* (Retallack et al., 2013). Other eukaryotes of comparable antiquity are 2.1 Ga intertidal-marine Franceville biota (El Albani et al., 2010, 2014, 2019), and perhaps 1.9 Ga lacustrine *Grypania* (Han and Runnegar, 1992; redated by Schneider et al., 2002).

Cyclomedusa is an extinct genus, proposed originally for fossils of Ediacaran age, and regarded as sea jellies (Sprigg, 1947; Glaessner and Wade, 1966). Like Ediacaran fossils, the Stirling Range discoids are positive impressions on the underside of covering sandstone, so

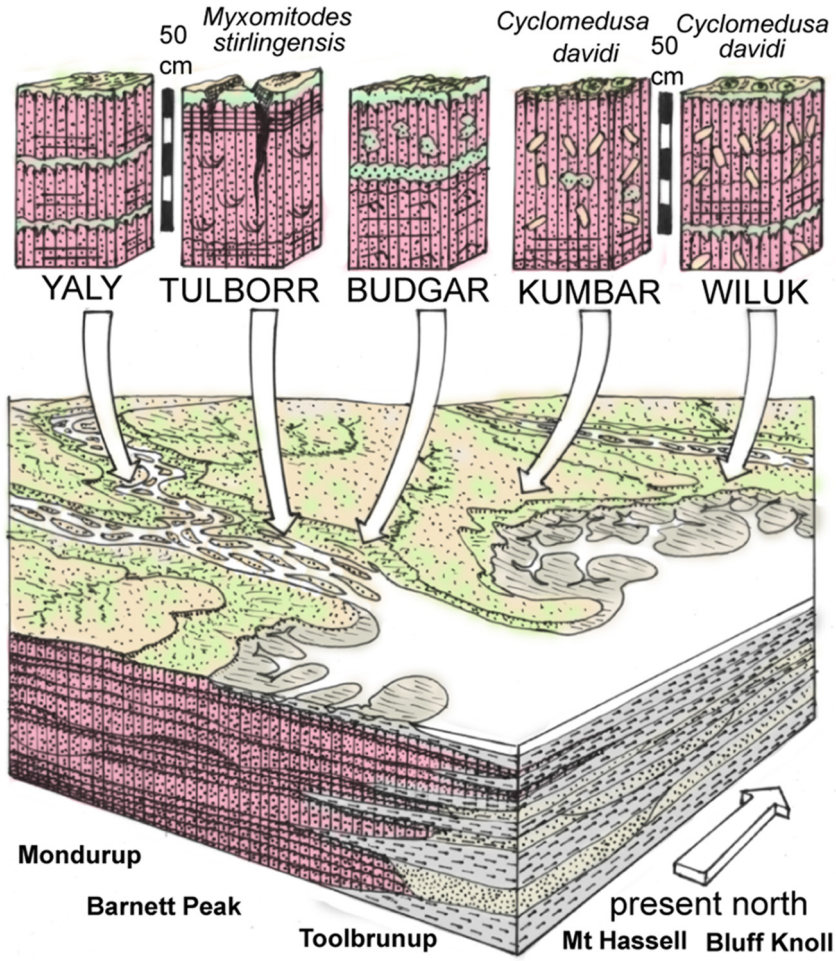

Fig. 12. Reconstructed Paleoproterozoic (1.9 Ga) paleoenvironment of Stirling Range Formation paleosols.

collapsed with compression (Retallack, 1994). This distinguishes them from other discoidal fossils such as *Aspidella*, which form negative impressions resistant to compaction on bed soles, and also have small patches of pleating not seen in *Cyclomedusa* (Retallack, 2016a). Also like the Ediacaran fossils, the Stirling Range fossils lack radial division, musculature, or gonads of sea jellies (Seilacher, 1992). Such amorphous discoids are now widely regarded as microbial colonies, like those of cyanobacteria (Grazhdankin and Gerdes, 2007). Although different bacteria make morphologically different colonies, local environment shapes them also (Ben-Jacob et al., 1994; Shapiro, 1995). Thus biological affinities of *Cyclomedusa* are unknown.

In addition to these problematic megafossils, the paleosols included microbially induced sedimentary structures (MISS of Noffke, 2009). Common on the paleosol surfaces are complex textures (Figs. 2A, 11G), that have been referred to “old elephant skin” and the ichnotaxon *Rivularites repertus* (Retallack, 2012, 2013a). “Old elephant skin” refers to a complex pattern of cracks, but there is also evidence of push-up ridges and domes, and thus alternating tension and compression. In describing desiccation-cracked sandstones like these (Fig. 2A–B), but from the Torridonian Supergroup (1 Ga) of Scotland, Prave (2002) emphasized how unusual it is for sand to crack as if it were clay. He argued that this was evidence that the soil was bound by a desiccation prone matrix, such as a biological soil crust. The term biological soil crust has been used for such communities in modern deserts, acknowledging that they include not only common cyanobacteria and other microbes, but lichens, liverworts, mosses, lycopsids and ephemeral angiosperms (Belnap, 2003). Here we use the term microbial earth (Retallack, 1992), because the paleosols were well drained (Section 6.3), as distinct from microbial mats, marsh, salt marsh and fen of waterlogged soils (Retallack, 2012). Microbial mats of local aquatic communities were also recognized in the Stirling Range Formation (Fig. 11F), as an ichnotaxon *Rugalichnus matthewi* (Stimson et al., 2017). Unlike terrestrial *Rivularites*, aquatic *Rugalichnus* has undulose detachments from the substrate (Retallack, 2012). Both cracked and undulose mats are widely recognized in Paleoproterozoic non-marine rocks (Eriksson et al., 2012; Simpson et al., 2013).

Also found in paleosols of the Stirling Range Formation were subvertical microfilamentous structures filled with red claystone (Fig. 6D), similar to lichen rhizines (Vogel, 1955; Poelt and Baumgärtner, 1964), slime molds (Martin et al., 1983; Stephenson and Stempen, 1994), and cyanobacterial ropes (Garcia-Pichel and Wojciechowski, 2009) common in biological soil crusts today (Belnap, 2003). It is not possible to distinguish between these alternatives given the indifferent quality of preservation of such tubular structures in paleosols (Driese et al., 1995; Retallack, 2008, 2009b).

7. Conclusions

This study addresses what, if anything, lived on land during the Paleoproterozoic. Besides cyanobacteria and fungi expected from other evidence, this may have included megascopic slime molds (Mycetozoa), which left fossil trails referred to the ichnotaxon *Myxomitodes stirlingensis* Bengtson et al. (2007). Mycetozoa are amoeba-like organisms living in soils as dispersed predators of bacteria and other microbes, but when food is short they coalesce into a slug-like body (grex), and migrate along the surface to a point where they form a column with

terminal sporangium. Also megascopic were discoidal fossils referred to *Cyclomedusa davidi* and here regarded as microbial colonies of uncertain biological affinity. Although the Stirling Range Formation with these controversial fossils has been considered marine to intertidal, our various analyses confirm that these ca. 1.9 Ga slime molds lived in soil like modern slime molds. Evidence for this conclusion comes from a variety of paleosols found along with the fossils: complex cracking patterns, sand crystals of gypsum, within-bed production of clay at expense of feldspar, alumina enrichment with cation depletion, loss of volume as well as weatherable cations, and light rare earth enrichment. Furthermore, the megafossils are found in association with wind ripples and other indications of non-marine habitats, in red beds of western outcrops of Stirling Range National Park, rather than in intertidal facies of eastern outcrops.

Acknowledgments

GJR thanks Kieran McNamara and Mike Shephard for permission to sample in Stirling Range National Park, Janet Bennett for mandatory *Phytophora* prevention training, John Abbott for local access, and Diane Retallack, Jeremy Retallack, and Ian Johnson for assistance in the field. John Donovan assisted with microprobe mapping. Mao Xuegang was supported by National Natural Science Foundation of China (Grant No. 41602184) and Natural Science Foundation of Fujian Province (2017J01655).

Appendix A. Supplementary data

Supplementary data to this article can be found online at https://doi.org/10.1016/j.palaeo.2019.109266.

References

Allen, J.R.L., 1963. Asymmetrical ripple marks and the origin of water-laid cosets of cross-strata. Geol. J. 3, 187–236.
Almohandis, A.A., 2002. Mineralogy and chemistry of desert roses, Ayn Dar area, Abqaiq, eastern province. Saudi Arabia. Qatar Univ. Sci. J. 22, 191–204.
Álvaro, J.J., Van Vliet-Lanoë, B., Vennin, E., Blanc-Valleron, M.M., 2003. Lower Cambrian paleosols from the Cantabrian Mountains (northern Spain): a comparison with Neogene–Quaternary estuarine analogues. Sediment. Geol. 163, 67–84.
Aubert, D., Stille, P., Probst, A., 2001. REE fractionation during granite weathering and removal by waters and suspended loads: Sr and Nd isotopic evidence. Geochim. Cosmochim. Acta 65, 387–406.
Bavinton, O.A., Taylor, S.R., 1980. Rare earth element geochemistry of Archean metasedimentary rocks from Kambalda. Western Australia. Geochim. Cosmochim. Acta 44, 639–648.
Belnap, J., 2003. Comparative structure of physical and biological soil crusts. In: Belnap, J., Lange, O.L. (Eds.), Biological Soil Crusts: Structure, Function and Management. Springer, Berlin, pp. 177–191.
Bengtson, S., Rasmussen, B., 2009. New and ancient trace makers. Science 323, 346–347.
Bengtson, S., Rasmussen, B., Krapež, B., 2007. The Paleoproterozoic megascopic Stirling biota. Paleobiology 33, 351–381.
Benison, K.C., Bowen, B.B., 2013. Extreme sulfur-cycling in acid brine lake environments of Western Australia. Chem. Geol. 351, 154–167.
Benison, K.C., Bowen, B.B., 2015. The evolution of end-member continental waters: the origin of acidity in southern Western Australia. GSA Today 25 (6), 1–10.
Benison, K.C., Bowen, B.B., Oboh-Ikuenobe, F.E., Jagniecki, E.A., LaClair, D.A., Story, S.L., Mormile, M.R., Hong, B.-Y., 2007. Sedimentology of acid saline lakes in southern Western Australia: newly described processes and products of an extreme environment. J. Sedim. Res. 77, 366–388.
Ben-Jacob, E., Schochet, O., Tenenbaum, A., Cohen, I., Czirok, A., Vicsek, T., 1994. Generic modelling of cooperative growth patterns in bacterial colonies. Nature 368, 46–49.
Bestland, E.A., Retallack, G.J., Rice, A.E., Mindszenty, A., 1996. Late Eocene detrital laterites in central Oregon: mass balance geochemistry, depositional setting and landscape evolution. Geol. Soc. Amer. Bull. 108, 285–302.
Black, L., Harris, L.B., Delor, C.P., 1993. Reworking of Archaean and Early Proterozoic components during a progressive, Middle Proterozoic tectonothermal event in the Albany Mobile Belt. Western Australia. Precambrian Res. 59, 95–123.
Bolhar, R., Van Kranendonk, M.J., Kamber, B.S., 2005. A trace element study of siderite jasper banded iron formation in the 3.45 Ga Warrawoona Group, Pilbara Craton: formation from hydrothermal fluids and shallow seawater. Precambrian Res. 137, 93–114.
Bonner, J.T., 2015. Cellular slime molds. Princeton University Press, Princeton (224 p.).
Boulter, C.A., 1979. On the production of two inclined cleavages during a single folding event, Stirling Range. SW Australia. J. Structural Geol. 1, 207–219.
Brimhall, G.H., Chadwick, O.A., Lewis, C.J., Compston, W., Williams, I.S., Danti, K.J., Dietrich, W.E., Power, M.E., Hendricks, D., Bratt, J., 1992. Deformational Mass Transport and Invasive Processes in Soil Evolution: Science 255, 695–702.
Bureau of Meteorology, 2016. Australian government website. http://www.bom.gov.au/climate/data/ (accessed April 7, 2016).
Chadwick, O.A., Brimhall, G.H., Hendricks, D.M., 1990. From a black to a gray box; a mass balance interpretation of pedogenesis. Geomorphology 3, 369–390.
Clark, D.J., Kinny, P.D., Post, N.J., Hensen, B.J., 1999. Relations between magnetism, metamorphism and deformation in the Fraser Complex. Western Australia: constraints from new SHRIMP U-Pb zircon geochronology. Australian J. Earth Sci. 46, 923–932.
Clark, D.J., Hensen, B.J., Kinny, P.D., 2000. Geochronological constraints for a two stage history of the Albany-Fraser Orogen. Western Australia. Precambrian Res. 102, 155–183.
Clauer, N., O'Neil, J.R., Bonnnot-Courtois, C., Holtzapfel, T., 1990. Morphological, chemical, and isotopic evidence for an early diagenetic evolution of detrital smectite in marine sediments. Clays Clay Minerals 38, 33–46.
Compton, J.S., White, R.A., Smith, M., 2003. Rare earth element behavior in soils and salt pan sediments of a semi-arid granitic terrain in the Western Cape, South Africa. Chem. Geol. 201, 239–255.
Cruse, T., Harris, L.B., 1994. Ediacaran fossil from the Stirling Range Formation. Western Australia. Precambrian Res. 67, 1–10.
Cruse, T., Harris, L.B., Rasmussen, B., 1993. The discovery of Ediacaran trace and body fossils in the Stirling Range Formation, Western Australia: implications for sedimentation and deformation during the "Pan-African" orogenic cycle. Australian J. Earth Sci. 40, 293–296.
Dawson, G.C., Krapež, B., Fletcher, I.R., McNaughton, N.J., Rasmussen, B., 2002. Did late Paleoproterozoic assembly of proto-Australia involve collisions between the Pilbara, Yilgarn and Gawler Cratons? Geochronological evidence from the Mt Barren Group in the Albany-Fraser Orogen of Western Australia. Precambrian Res. 118, 195–220.
Dawson, G.C., Krapež, B., Fletcher, I.R., McNaughton, N.J., Rasmussen, B., 2003. 1.3 Ga thermal metamorphism in the Albany-Fraser Orogen of Western Australia: consequences of collision or regional heating by dyke swarms? Geol. Soc. London J. 160, 29–37.
de Sá Paye, H., de Mello, J.W., de Magalhães Mascarenhas, G.R.L., Gasparon, M., 2016. Distribution and fractionation of the rare earth elements in Brazilian soils. J. Geochem. Explor. 161, 27–41.
Douglas, W., 1991. Nungar-English, English-Nungar Dictionary. W.H. Atkins Memorial, Wellington Mills (35 pp.).
Driese, S.G., 2004. Pedogenic translocation of Fe in modern and ancient Vertisols and implications for interpretations of the Hekpoort Paleosol (2.25 Ga). J. Geol. 112, 543–560.
Driese, S.G., Simpson, E., Ericksson, K.A., 1995. Redoximorphic paleosols in alluvial and lacustrine deposits, 1.8 Ga Lochness Formation, Mt Isa: pedogenic processes and implications for paleoclimate. J. Sedim. Res. A66, 58–70.
Droser, M.L., Gehling, J.G., Dzaugis, M.E., Kennedy, M.J., Rice, D., Allen, M.F., 2014. A new Ediacaran fossil with a novel sediment displacive life habit. J. Paleontol. 88, 145–151.
Eberl, D.D., Srodon, J., Kralik, M., Taylor, B.E., Peterman, Z.E., 1990. Ostwald ripening of clays and metamorphic minerals. Science 248, 474–477.
El Albani, A., Bengtson, S., Canfield, D.E., Bekker, A., Macchiarelli, R., Mazurier, A., Hammarlund, E.U., Boulvais, P., Dupuy, J.J., Fontaine, C., Fürsich, F.T., 2010. Large colonial organisms with coordinated growth in oxygenated environments 2.1 Gyr ago. Nature 466, 100–104.
El Albani, A., Bengtson, S., Canfield, D.E., Riboulleau, A., Bard, C.R., Macchiarelli, R., Pemba, L.N., Hammarlund, E., Meunier, A., Mouélé, I.M., Benzerara, K., 2014. The 2.1 Ga old Francevillian biota: biogenicity, taphonomy and biodiversity. PLoS One 9(6), e99438.
El Albani, A., Mangano, M.G., Buatois, L.A., Bengtson, S., Riboulleau, A., Bekker, A., Konhauser, K., Lyons, T., Rollion-Bard, C., Bankole, O., Baghekema, S.G.L., Meunier, A., Trentesaux, A., Mazurier, A., Aubineau, J., Laforest, C., Fontaine, C., Recourt, P., Fruh, E.C., Macchiarelli, R., Reynaud, J.Y., François Gauthier-Lafayek, F., Canfield, D.E., 2019. Organism motility in an oxygenated shallow-marine environment 2.1 billion years ago. U.S. Nat. Acad. Sci. Proc. 116, 3431–3436.
Eriksson, P.G., Bartman, R., Catuneanu, O., Mazumder, R., Lenhardt, N., 2012. A case study of microbial mat-related featrues in coastal epeiric sndstonesfrom the Paleoproterozoic Pretaoria Group (Transval Supergroup, Kaapvaaal Craton, South Africa; the effect of preservation (reflecting sequence stratigraphic models) on the relationship between mat features and inferred paleoenvironment. Sedim. Geol. 263–264, 67–75.
Evans, D.A.D., 2009. The palaeomagnetically viable, long-lived and all-inclusive Rodinia supercontinent reconstruction. In: Murphy, J.B., Keppie, J.D., Hynes, A.J. (Eds.), Ancient Orogens and Modern Analogues. Geol. Soc. London Spec. Publ 327. pp. 371–404.
Ewing, S.A., Sutter, B., Owen, J., Nishiizumi, K., Sharp, W., Cliff, S.S., Perry, K., Dietrich, W., McKay, C.P., Amundson, R., 2006. A threshold in soil formation at Earth's arid-hyperarid transition. Geochim. Cosmochim. Acta 70, 5291–5322.
Fedonkin, M.A., Gehling, J.G., Grey, K., Narbonne, G.M., Vickers-Rich, P., 2007. The rise of animals. Johns Hopkins University Press, Baltimore (326 pp.).
Fiorella, R.P., Sheldon, N.D., 2017. Equable end Mesoproterozoic climate in the absence of high CO_2. Geology 45, 231–234.
Foden, J.D., Nesbitt, R.W., Rutland, R.W.R., 1984. The geochemistry and crustal origin of the Archaean acid intrusive rocks of the Agnew Dome, Lawlers. Western Australia. Precambrian Res. 23, 247–271.
Food and Agriculture Organization, 1974. Soil Map of the World, 1:500,000. I. Legend,

UNESCO, Paris (59 pp).
Food and Agriculture Organization, 1978. Soil Map of the World, 1:500,000. X. Australasia. UNESCO, Paris (221 pp.).
Gallagher, T.M., Sheldon, N.D., 2013. A new paleothermometer for forest paleosols and its implications for Cenozoic climate. Geology 41, 647–651.
Garcia-Pichel, F., Wojciechowski, M.F., 2009. The evolution of a capacity of build extracellular ropes enabled filamentous cycanobacteria to colonize highly erodible substrates. PLoS One 4, e7801.
Glaessner, M.F., Wade, M., 1966. The late Precambrian fossils from Ediacara, South Australia. Palaeontology 9, 599–628.
Grandstaff, D.E., Edelman, M.J., Foster, R.W., Zbinden, E.M., Kimberley, M.M., 1986. Chemistry and mineralogy of Precambrian paleosols at the base of the Dominion and Pongola Groups (Transvaal, South Africa). Precambrian Res. 32, 97–131.
Grazhdankin, D., Gerdes, H., 2007. Ediacaran microbial colonies. Lethaia 30, 201–210.
Han, T.-M., Runnegar, B., 1992. Megascopic eukaryotic algae from the 2.1-billionyear-old Negaunee Iron-Formation. Science 257, 232–235.
Harris, L.B., 1994. Neoproterozoic sinistral displacement along the Darling Mobile Belt, western Australia, during Gondwanaland assembly. Geol. Soc. London J. 151, 901–904.
Harris, L.B., Beeson, J., 1993. Gondwanaland significance of Lower Palaeozoic deformation in central India and SW Western Australia. Geol. Soc. London J. 150, 811–814.
Harris, L.B., Li, Z.-X., 1995. Palaeomagnetic dating and tectonic significance of dolerite intrusions in the Albany Mobile Belt. Western Australia. Earth Planet. Sci. Lett. 131, 143–164.
Hocking, R.M., 1991. The Silurian Tumblagooda Sandstone, Western Australia. Geol. Surv. Western Australia Rept 27, 1–125.
Hughes, I., Hase, I.P.A., 2010. Measurements and Their Uncertainties: A Practical Guide to Modern Error Analysis. Oxford Univ, Press, Oxford (136 pp).
Hunter, R.E., 1977. Basic types of stratification in small eolian dunes. Sedimentology 24, 361–387.
Isbell, R.F., 1996. The Australian Soil Classification. C.S.I.R.O, Collingwood (152 pp.).
Jafarzadeh, A.A., Burnham, C.P., 1992. Gypsum crystals in soils. J. Soil Sci. 43, 409–420.
Kasting, J., Kirschvink, J., 2012. Evolution of a habitable planet. In: Impey, C., Lunine, J., Funes, J. (Eds.), Frontiers of Astrobiology. Cambridge Univ. Press, New York, pp. 115–131.
Kump, L.R., 2008. The rise of atmospheric oxygen. Nature 451, 277–278.
Kurtz, A.C., Derry, L.A., Chadwick, O.A., 2001. Accretion of Asian dust to Hawaiian soils: isotopic, elemental, and mineral mass balances. Geochim. Cosmochim. Acta 65, 1971–1983.
Liu, Y., Li, Z.X., Pisarevsky, S., Kirscher, U., Mitchell, R.N., Stark, J.C., 2019. Palaeomagnetism of the 1.89 Ga Boonadgin dykes of the Yilgarn Craton: possible connection with India. Precambrian Res. https://doi.org/10.1016/j.precamres.2018.05.021.
Lyons, T.W., Reinhard, C.T., Planavsky, N.J., 2014. The rise of oxygen in Earth's early ocean and atmosphere. Nature 506, 307–315.
Mao, X.-G., Retallack, G.J., 2019. Late Miocene drying of central Australia. Palaeogeogr. Palaeoclimatol. Palaeoecol. 514, 292–304.
Martin, G.W., Alexopoulos, C.J., Farr, M.L., 1983. The Genera of Myxomycetes. University of Iowa Press, Iowa City (561 pp.).
McBride, E.F., 1989. Quartz cement in sandstones: a review. Earth Sci. Rev. 26, 69–112.
McKenzie, N., Jacquier, D., Isbell, R., Brown, K., 2004. Australian Soils and Landscapes. CSIRO, Melbourne (416 pp).
McQuarrie, N., Tobgay, T., Long, S.P., Reiners, P.W., Cosca, M.A., 2014. Variable exhumation rates and variable displacement rates: documenting recent slowing of Himalayan shortening in western Bhutan. Earth Planet. Sci. Lett. 386, 161–174.
Merritts, D.J., Chadwick, O.A., Hendricks, D.M., Brimhall, G.H., Lewis, C.J., 1992. The mass balance of soil evolution on late Quaternary marine terraces, Northern California. Geol. Soc. Amer. Bull. 104, 1456–1470.
Miller, M.C., Komar, P.D., 1980. A field investigation of the relationship between oscillation ripple spacing and the near-bottom water orbital motions. J. Sedim. Res. 50, 183–191.
Mitchell, R.L., Sheldon, N.D., 2009. Weathering and paleosol formation in the 1.1 Ga Keweenawan Rift. Precambrian Res.168, 271-283.
Muhling, P.C., Brakel, A.T., 1985.Mount Barker-Albany 1:250,000 Geological Series – Explanatory Notes. Geological Survey of Western Australia, Perth (21 pp.).
Murphy, C.P., 1983. Counting pores and illuvial clay in thin section. Geoderma 31, 133–150.
Nabhan, S., Luber, T., Scheffler, F., Heubeck, C., 2016. Climatic and geochemical implications of Archean pedogenic gypsum in the Moodies group (~3.2 Ga), Barberton Greenstone Belt, South Africa. Precambrian Res. 275, 119–134.
Nance, W.B., Taylor, S.R., 1976. Rare earth element patterns and crustal evolution—I. Australian post-Archean sedimentary rocks. Geochim. Cosmochim. Acta 40, 1539–1551.
Navarro-González, R., Rainey, F.A., Molina, P., Bagalay, D.R., Hollen, B.J., de la Rosa, J., Small, A.M., Quinn, R.C., Grunthaner, F.J., Caceres, L., Gomez-Silva, B., McKay, C.P., 2003. Mars-like soils in the Atacama Desert, Chile, and the dry limit of microbial life. Science 302, 1018–1021.
Nesbitt, H.W., Young, G.M., 1989. Formation and diagenesis of weathering profiles. J. Geol. 97, 129–147.
Noffke, N., 2008. A turbulent lifestyle; microbial mats on Earth's sandy beaches, today and 3 billion years ago. GSA Today 18 (10), 4–8.
Noffke, N., 2009. The criteria for the biogenicity of microbially induced sedimentary structures (MISS) in Archaean and younger, sandy deposits. Earth Sci. Rev. 96, 173–180.
Novoselov, A.A., de Souza Filho, C.R., 2015. Potassium metasomatism of Precambrian paleosols. Precambrian Res. 262, 67–83.
Ohmoto, H., Watanabe, Y., Lasaga, A.C., Naraoka, H., Johnson, I., Brainard, J., Chorney, A., 2014. Oxygen, iron and sulfur geochemical cycles on the early Earth: problems and contradictions. In: Shaw, G.H. (Ed.), Earth's Early Atmosphere and Surface Environment. Geol. Soc. Amer. Spec. Pap, vol. 504. pp. 55–95.
Óskarsson, B.V., Riishuus, M.S., Arnalds, O., 2012. Climate-dependent chemical weathering of volcanic soils in Iceland. Geoderma 189–190, 635–651.
Planavsky, N.J., Cole, D.B., Isson, T.T., Reinhard, C.T., Crockford, P.W., Sheldon, N.D., Lyons, T.W., 2018. A case for low atmospheric oxygen levels during Earth's middle history. Emerging Topics Life Sci. 2, 149–159.
Poelt, J., Baumgärtner, H., 1964, Über Rhizinenstränge bei placodialen Flechten. Österreich Bot. Zeit. 111, 1–18.
Prave, A.R., 2002. Life on land in the Proterozoic: evidence from the Torridonian rocks of northwest Scotland. Geology 30, 811–814.
Ramakrishnan, D., Tiwari, K.C., 1999. REE chemistry of arid zone calcrete profiles—a case study from the Thar Desert. India. Turkish J. Earth Sci. 7, 97–104.
Rasmussen, B., Fletcher, I.R., 2004. Zirconolite: a new U-Pb chronometer for mafic igneous rocks. Geology 32, 785–788.
Rasmussen, B., Muhling, J., 2007. Monazite begets monazite: evidence for dissolution of detrital monazite and reprecipitation of syntectonic monazite during low-grade regional metamorphism. Contrib. Mineral. Petrol.154, 675–689.
Rasmussen, B., Muhling, J.R., 2019. Syn-tectonic hematite growth in Paleoproterozoic Stirling Range “red beds”, Albany-Fraser Orogen. Australia: Evidence for oxidation during late-stage orogenic uplift. Precambrian Res. 321, 54–63.
Rasmussen, B., Bengtson, S., Fletcher, I.R., McNaughton, N.J., 2002a. Discoidal impressions and trace-like fossils more than 1200 million years old. Science 296, 1112–1115.
Rasmussen, B., Bengtson, S., Fletcher, I.R., McNaughton, N.J., 2002b. Ancient animals or something else entirely? Science 298, 58–59.
Rasmussen, B., Fletcher, I.R., Bengtson, S., McNaughton, N.J., 2004. SHRIMP U-Pb daring of diagenetic xenotime in the Stirling Range Formation, Western Australia: 1.8 billion year minimum age for the Stirling biota. Precambrian Res. 133, 329–337.
Renaut, R.W., Tiercelin, J.-J., 1994. Lake Bogoria, Kenya Rift Valley - a sedimentological overview. In: Renaut, R.W., Last, W.M. (Eds.), Sedimentology and Geochemistry of Modern and Ancient Saline Lakes. Soc. Sediment. Geol. Spec. Publ, vol. 50. pp. 101–124.
Retallack, G.J., 1991. Untangling the effects of burial alteration and ancient soil formation: Ann. Rev. Earth Planet. Sci. 19, 183–206.
Retallack, G.J., 1992. What to call early plant formations on land. Palaios 7, 508–520.
Retallack, G.J., 1994. Were the Ediacaran fossils lichens? Paleobiology 20, 523–544.
Retallack, G.J., 1997. A colour guide to paleosols. Wiley, Chichester (346 pp).
Retallack, G.J., 2001. Soils of the Past. Blackwell, Oxford (404 pp).
Retallack, G.J., 2005. Pedogenic carbonate proxies for amount and seasonality of precipitation in paleosols. Geology 33, 333–336.
Retallack, G.J., 2008. Cambrian paleosols and landscapes of South Australia. Australian J. Earth Sci. 55, 1083–1106.
Retallack, G.J., 2009a. Early Paleozoic pedostratigraphy and global events in Australia. Australian J. Earth Sci. 56, 569–584.
Retallack, G.J., 2009b. Cambrian-Ordovician non-marine fossils from South Australia. Alcheringa 33, 355–391.
Retallack, G.J., 2011. Neoproterozoic glacial loess and limits to snowball Earth. Geol. Soc. London J. 168, 1–19.
Retallack, G.J., 2012. Criteria for distinguishing microbial mats and earths. In: Noffke, N., Chafetz, H. (Eds.), Microbial Mats in Siliciclastic Sediments. Soc. Econ. Paleont. Mineral. Spec. Pap, vol. 101. pp. 136–152.
Retallack, G.J., 2013a. Ediacaran life on land. Nature 493, 89–92.
Retallack, G.J., 2013b. Comment on “Trace fossil evidence for Ediacaran bilaterian animals with complex behaviors” by Chen et al. [Precambrian Res. 224 (2013) 690-701]. Precambrian Res. 231, 383–385.
Retallack, G.J., 2014a. Paleosols and paleoenvironments of early Mars. Geology 42, 755–758.
Retallack, G.J., 2014b. Precambrian life on land. The Palaeobotanist 63, 1–15.
Retallack, G.J., 2016a. Ediacaran sedimentology and paleoecology of Newfoundland reconsidered. Sedim. Geol. 333, 15–31.
Retallack, G.J., 2016b. Field and laboratory tests for recognition of Ediacaran paleosols. Gondwana Res. 36, 94–110.
Retallack, G.J., 2018. Oldest recognized paleosols on Earth, Panorama Formation (3.46 Ga), Western Australia. Palaeogeogr. Palaeoclim. Palaeoec. 489, 230–248.
Retallack, G.J., Huang, C.-M., 2010. Depth to gypsic horizon as a proxy for paleoprecipitation in paleosols of sedimentary environments. Geology 38, 403–406.
Retallack, G.J., Mindszenty, A., 1994. Well preserved Late Precambrian paleosols from northwest Scotland. J. Sedim. Res. A64, 264–281.
Retallack, G.J., Noffke, N., 2019. Are there ancient soils in the 3.7 Ga Isua Greenstone Belt, Greenland? Palaeogeogr. Palaeoclim. Palaeoec. 514, 18–30.
Retallack, G.J., Krull, E.S., Thackray, G.D., Parkinson, D., 2013. Problematic urn-shaped fossils from a Paleoproterozoic (2.2 Ga) paleosol in South Africa. Precambrian Res. 235, 71–87.
Retallack, G.J., Krinsley, D.H., Fischer, R., Razink, J.J., Langworthy, K., 2016. Archean coastal-plain paleosols and life on land. Gondwana Res. 40, 1–20.
Robbins, L.J., Funk, S.P., Flynn, S.L., Warchola, T.J., Li, Z., Lalonde, S.V., Rostron, B.J., Smith, A.J., Beukes, N.J., de Kock, M.O., Heaman, L.M., 2019. Hydrogeological constraints on the formation of Palaeoproterozoic banded iron formations. Nat. Geosci. 12, 558–563.
Schneider, D.A., Bickford, M.E., Cannon, W.F., Schulz, K.J., Hamilton, M.A., 2002. Age of volcanic rocks and syndepositional iron formations. Marquette Range Supergroup: implications for the tectonic setting of Paleoproterozoic iron formations of the Lake

Superior region. Canadian J. Earth Sci. 39, 999–1012.
Seilacher, A., 1992. Vendobionta and Psammocorallia: lost constructions of Precambrian evolution. J. Geol. Soc. Lond. 149, 607–613.
Seilacher, A., 2007. Trace Fossil Analysis. Springer, Berlin (226 pp.).
Setti, M., Marinoni, L., López-Galindo, L., 2004. Mineralogical and geochemical characteristics (major, minor, trace elements and REE) of detrital and authigenic clay minerals in a Cenozoic sequence from Ross Sea, Antarctica. Clay Mineralogy 39, 405–421.
Shapiro, J.A., 1995. The significances of bacterial colony patterns. Bioessays 17, 597–607.
Sheldon, N.D., 2003. Pedogenesis and geochemical alteration of the Picture Gorge Subgroup, Columbia River Basalt, Oregon. Geol. Soc. Amer. Bull.115, 1377–1387.
Sheldon, N.D., 2006. Precambrian paleosols and atmospheric CO_2 levels. Precambrian Res. 147, 148–155.
Sheldon, N.D., Retallack, G.J., 2001. Equation for compaction of paleosols due to burial. Geology 29, 247–250.
Sheldon, N.D., Retallack, G.J., Tanaka, S., 2002. Geochemical climofunctions from North American soils and application to paleosols across the Eocene-Oligocene boundary in Oregon. J. Geol. 110, 687–696.
Simpson, E.L., Heness, E., Bumby, A., Eriksson, P.G., Eriksson, K.A., Hilbert-Wolf, H.L., Sarah Linnevelt, S., Malenda, H.F., Modungwa, T., Okafor, O.J., 2013. Evidence for 2.0 Ga continental microbial mats in a paleodesert setting. Precambrian Res. 237, 36–50.
Soil Survey Staff, 2014. Keys to Soil Taxonomy. Natural Resource Conservation Service, Washington (600 pp.).
Som, S.M., Catling, D.C., Harnmeijer, J.P., Polivka, P.M., Buick, R., 2012. Air density 2.7 billion years ago limited to less than twice modern levels by fossil raindrop imprints. Nature 484, 359–362.
Som, S.M., Buick, R., Hagadorn, J.W., Blake, T.S., Perreault, J.M., Harnmeijer, J.P., Catling, D.C., 2016. Earth's air pressure 2.7 billion years ago constrained to less than half of modern levels. Nat. Geosci. 9, 448–452.
Sprigg, R.C., 1947. Early Cambrian (?) jellyfishes from the Flinders Ranges. South Australia. Roy. Soc.South Australia Trans. 71, 212–222.
Stace, H.C.T., Hubble, G.T., Brewer, R., Northcote, K.H., Sleeman, J.R., Mulcahy, M.J., Hallsworth, E.G., 1968. A Handbook of Australian Soils. Rellim, Adeladie (435 pp.)
Stephenson, S.L., Stempen, H., 1994. Myxomycetes: A Handbook of Slime Molds. Timber Press, Portland (183 pp.).
Stimson, M.R., Miller, R.F., MacRae, R.A., Hinds, S.J., 2017. An ichnotaxonomic approach to wrinkled microbially induced sedimentary structures. Ichnos 24, 291–316.
Sugahara, H., Sugitani, K., Mimura, K., Yamashita, F., Yamamoto, K., 2010. A systematic rare-earth elements and yttrium study of Archean cherts at the Mount Goldsworthy greenstone belt in the Pilbara Craton: implications for the origin of microfossil bearing black cherts. Precambrian Res. 177, 73–87.
Trail, D., 2018. Redox-controlled dissolution of monazite in fluids and implications for phase stability in the lithosphere. Am. Mineral. 103, 453–461.
Turek, A., Stephenson, N.C.N., 1966. The radiometric age of the Albany granite and Stirling Range Beds, southwest Australia. Geol. Soc. Australia J. 13, 449–456.
Vepraskas, M.J., Sprecher, S.W., 1997. Summary. In: Vepraskas, M.J., Sprecher, S.W. (Eds.), Aquic Conditions and Hydric Soils: The Problem Soils. Soil Sci. Soc. Amer. Spec. Publ 150. pp. 153–156.
Vogel, S., 1955. Niedere “Fensterpflanzen”: in der südafrikanischen Wüste. Beitrage Biologie Pflanzen 31, 45–135.
Weinberger, R., 2001. Evolution of polygonal patterns in stratified mud during desiccation; the role of flaw distribution and layer boundaries. Geol. Soc. Amer. Bull. 113, 20–31.
Williams, G.E., Schmidt, P.W., Clark, D.A., 2004. Palaeomagnetism of iron-formation from the late Palaeoproterozoic Frere Formation, Earaheedy Basin. Western Australia: palaeogeographic and tectonic implications. Precambrian Res. 128, 367–383.
Woolnough, W.G., 1920. A geological reconnaissance of the Stirling Ranges of Western Australia. Roy. Soc. New South Wales J. Proc. 54, 79–112.
Wordsworth, R., Pierrehumbert, R., 2013. Hydrogen-nitrogen greenhouse warming in Earth's early atmosphere. Science 339, 64–67.
Ziegenbalg, S.B., Brunner, B., Rouchy, J.M., Birgel, D., Pierred, C., Böttcher, M.E., Caruso, A., Immenhauser, A., Peckmann, J., 2010. Formation of secondary carbonates and native sulfur in sulfate-rich Messinian strata. Sicily. Sedim. Geol. 227, 37–50.